Lawrence Berkeley Laboratory
UNIVERSITY OF CALIFORNIA

Physics Division

Presented at a Round Table Discussion at the 8th International Conference on Physics in Collision, Capri, Italy, October 19–21, 1988, and to be published in the Proceedings

The Search for the Top Quark

A. Barbaro-Galtieri

March 1989

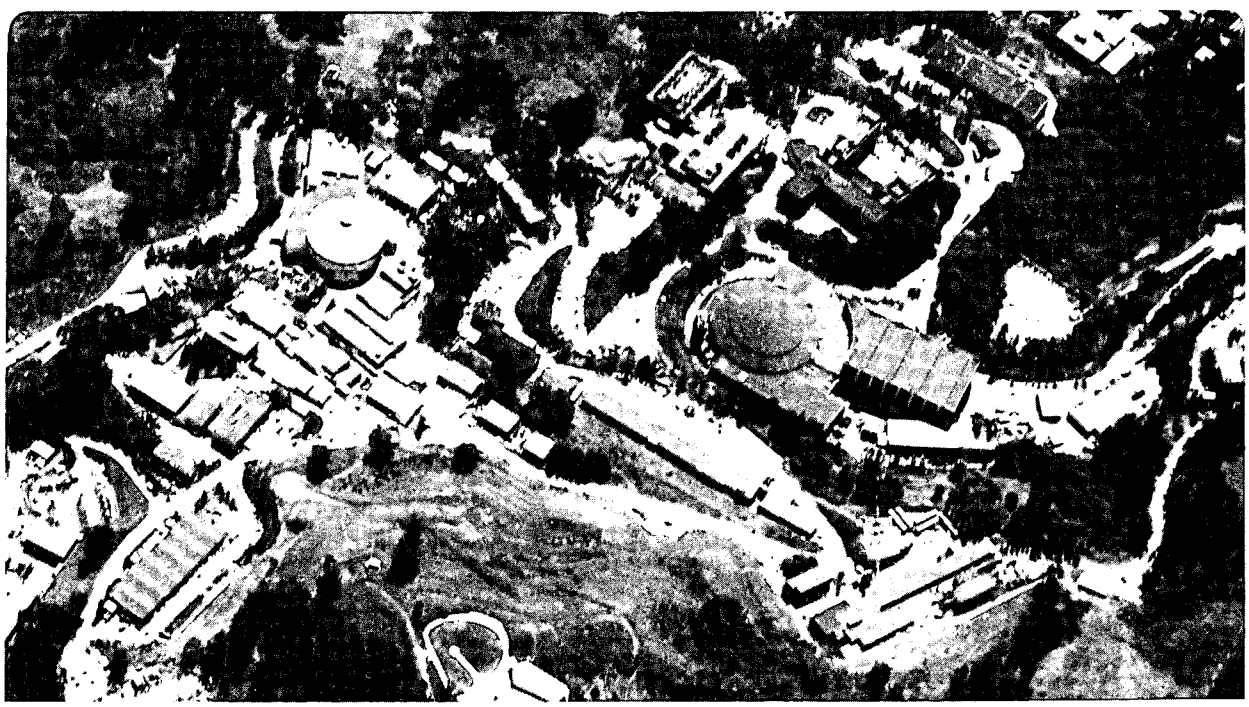

Prepared for the U.S. Department of Energy under Contract Number DE-AC03-76SF00098.

DISCLAIMER

LBL-26917

The Search for the Top Quark[1]

A. Barbaro-Galtieri
Physics Division
Lawrence Berkeley Laboratory
1 Cyclotron Road, Berkeley, CA 94720

with the participation of:

R. Felst
DESY, Notkestrasse 85, D-2000 Hamburg-52, West Germany

J. Dorfan
SLAC, P.O. Box 4349, Stanford, CA 94305

A. Blondel
CERN, CH-1211 Geneva-23, Switzerland

J. Schacher
Laboratorium für Hochenergiephysik, Universität Bern
Sidlerstrasse 5, CH 3012 Bern, Switzerland

D. Denegri
CERN, CH-1211 Geneva 23, Switzerland and
CEN-Saclay, BP No. 2, F-91191, Gif-sur-Yvette, France

March 1989

Round Table Discussion at the
8th International Conference on "Physics in Collision"
Capri, Italy
October 19-21, 1988

---

[1]This work is supported in part by the Director, Office of Energy Research, Office of High Energy and Nuclear Physics, Division of High Energy Physics of the U.S. Department of Energy under Contract DE-AC03-76SF00098.

1. Introduction

The top quark is an important ingredient of the standard model. It is the last missing member of the 3 generations of quarks and its mass is highly correlated with a number of parameters of the model. The u, d, s quarks have been "discovered" in the '60's when the eight-fold way and the quark model were hypothesized[1]; the charm quark was inferred from the J/ψ discovery[2] in 1974 and later detected in charm particles[3], the b quark was discovered in 1977 via the production of the Υ states.[4]

The search for the top quark since 1977 has provided only upper limits. The most recent are:

$m_t > 27.4$ GeV e^+e^- collider, Tristan[5]
$m_t > 41$ GeV UA1 collider at the Spp̄S[6,7]

The standard model imposes upper and lower limits on the mass of the top. A lower limit is obtained through the constrainsts of the so-called Cabibbo-Kobayashi-Maskawa[8,9] mixing matrix. Recent measurements of B° - $\bar{B}^\circ$ mixing[10] and a non-zero value for the CP violation parameter ε'/ε[11] have allowed detailed analyses of the relation of the top mass to these parameters. Predictions depend upon strong interaction corrections to the matrix elements, that introduce some uncertainties.

This type of analysis has been made by many groups[12]. The lower mass limit for the top is found to be in the range:

$$m_t > 50 - 55 \text{ GeV}$$

As an illustration, Fig. 1, taken from Buras and Gerard[13], shows the allowed region of top masses as a function of ε'/ε, the measured B° - $\bar{B}^\circ$ mixing and the parameter $R = \Gamma(b \to ue\nu)/\Gamma(b \to ce\nu)$. A detailed discussion of this subject can be found in the report by K. Kleinknecht in these Proceedings.

An upper limit on the top mass has been derived by Amaldi et al.[14] by a global analysis, within the standard model, of most existing weak neutral current measurements and the W and Z masses. Electroweak radiative corrections were included. Also statistical, systematic and theoretical uncertainties were combined, and available error correlations were taken into account. The limit, which depends on the Higgs mass, is

$$m_t < 180 \text{ GeV}, \qquad \text{for } m_H < 100 \text{ GeV}$$

Fig. 2 shows the allowed region of m_t versus the value of $\sin^2\theta_W$. The global fit gives $\sin^2\theta_W = 0.230 \pm .005$. A discussion of this analysis can be found in the report of K. Winter in these Proceedings.

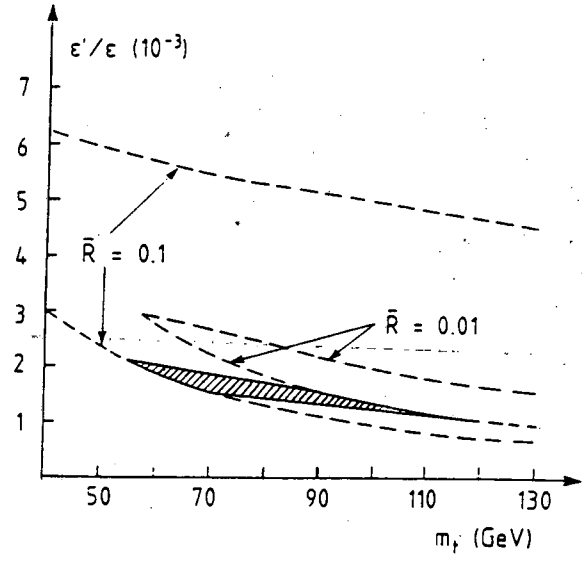

Fig. 1: Constraints to the top mass from the standard model obtained in the analysis of Buras and Gerard (Ref.13). The ratio ε'/ε as a function of m_t for $\tau(B) = 1.1 \times 10^{-12}$ s and two extreme values R=0.01 and R=0.1. The dashed lines represent the values consistent with ε_{exp} but forbidden by B^o-$\bar{B}^o$ mixing. Only the curves contained in the shaded region are allowed by both ε_{exp} and B^o-$\bar{B}^o$ mixing. Here:
$R = \Gamma(b \to u e \nu)/\Gamma(b \to c e \nu)$.

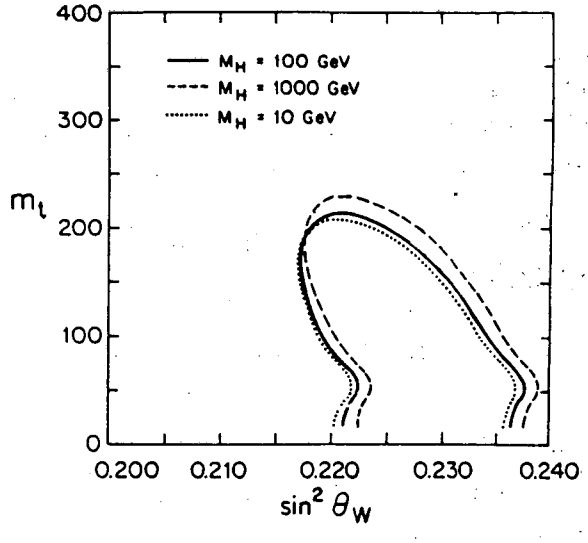

Fig. 2: Constraint on the top mass from the analysis of Amaldi et al. (Ref. 14) of weak neutral current data and Z and W masses, including radiative corrections. Allowed regions of $\sin^2\theta_W$ and m_t for different Higg masses are shown. The global fit gives $\sin^2\theta_W = 0.230 \pm 0.005$.

2. Top Search in The Near Future: General Remarks

Since the mass of the top is reported to be greater than 41 GeV, only colliders have an opportunity to reach such energies. In this Round Table we have representatives of the various colliders now working and of the ones scheduled to take data within 1990. Strategies to separate signal from background for a top search depend upon the type of collider and on the top mass.

a. e^+e^- colliders

SLC and LEP are scheduled to take data within the next year. The production cross section for top pairs, apart from QCD corrections, are well known. The main strategies are well understood: study of high $P_\perp$ leptons and event topology.

b. $\bar{p}p$ colliders

Both the Sp$\bar{p}$S and the Tevatron colliders are now taking data. Here the production cross sections are calculable via QCD, but there are many uncertainties, as we will see in the next section. Strategies include: study of isolated leptons, jet counting and event topologies. Major backgrounds are from b pair production and W + jets.

c. e p colliders

HERA is expected to turn on in 1990. Here uncertainties in QCD calculations play a role in evaluating production cross sections. Strategies are similar to those used for the other colliders.

2.1 Heavy Quark Production in Hadronic Collisions

Uncertainties on the cross sections for b pair and top pair productions are common to three experiments (UA2', UA1, CDF). To avoid duplication they will be discussed here.

Next-to-leading order QCD calculations for heavy quark production have been done by Nason, Dawson and Ellis[15]. Over 300 diagrams of order α^3_s have been calculated, so that cancellation of collinear and soft divergencies were properly taken care of. The resulting cross sections, however, are highly dependent on different quantities like the parton structure functions (especially the gluon), the choice of the renormalization and factorization scale μ, the choice of Λ (α_s is a function of μ^2/Λ^2), and the heavy quark mass.

Fig. 3 shows, as a function of the quark mass, the ratio of cross sections

$$K = \frac{\sigma\,[O\,(\alpha_s^3)]}{\sigma\,[O\,(\alpha_s^2)]}$$

for the EHLQ1 structure functions and various choices of μ. The K factor appears to be quite large at the b mass, and has a large dependence on the choice of scale. For top masses above 40 GeV, the K factor is definitively smaller than that for the bottom quark.

Altarelli et al.[7] in conjunction with the results of Nason et al., have used a recent set of structure functions, DFLM[16]. They have evaluated the range of

uncertainties due to choices of scale, Λ, and quark mass. The QCD evolution of the

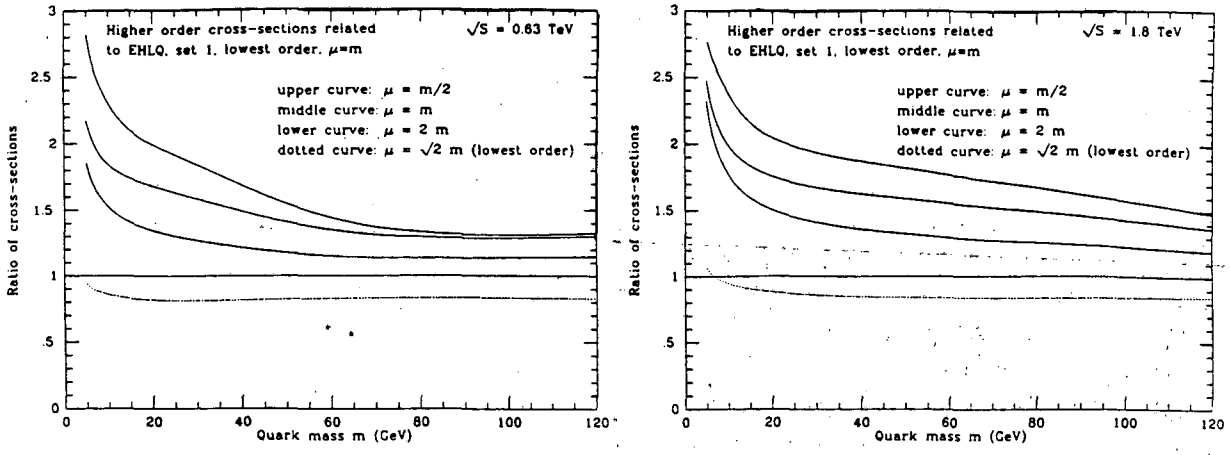

Fig. 3: The ratio of the $O(\alpha_s^3)$ heavy quark cross section to the $O(\alpha_s^2)$ cross section as a function of the heavy quark mass.[15] The EHLQ1 set of structure functions are used. Two different choices of scale are shown for the lowest order and three for the higher order. The two graphs are for CERN and FNAL energies.

DFLM structure functions is performed at next-to-leading order, and in addition, Λ can be varied in the QCD evolution. They find that the top cross section uncertainties are of the order of 30%, whereas the bottom cross section uncertainties are much larger. Fig. 4 shows the top cross section as a function of top mass, as calculated by these authors.[7]

The large uncertainties in the b cross section can be seen in Fig. 5 at 0.63 and 1.8 TeV. The curves have been calculated by Ellis[17], using the same method as Altarelli et al.[7] and the DFLM structure functions. Clearly the K factor is larger than 2 everywhere, for both energies. In calculating the b background to top, these uncertainties have to be taken into account. The UA1 collaboration has measured the b pair cross section to be[18]

$$\sigma(p\bar{p} \rightarrow b\bar{b} + x) = 10.2 \pm 3.3\ \mu b \qquad \text{UA1 Collaboration}$$

This result can be accommodated within the theoretical predictions.[7]

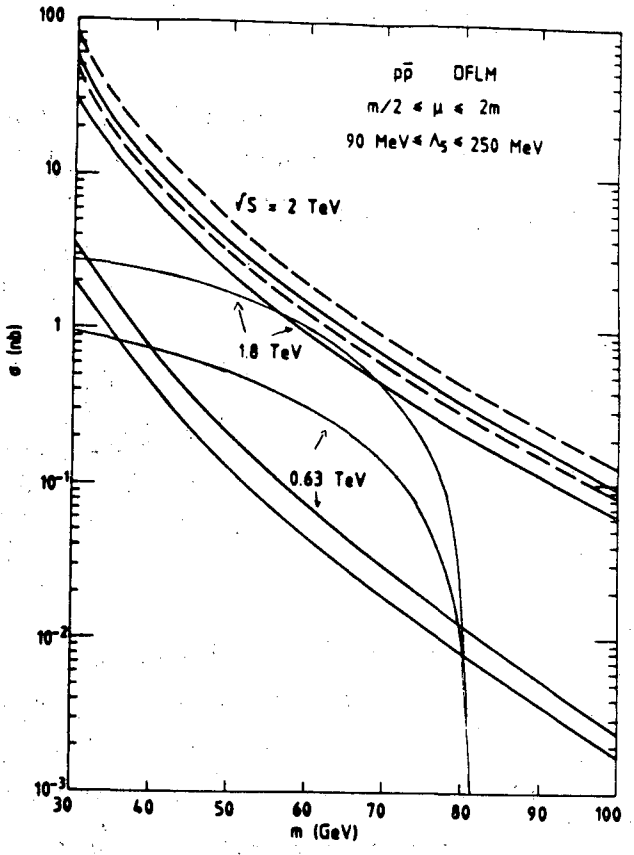

Fig. 4: The top pair production cross section versus top mass, as calculated by Altarelli et al[7], using the results of Nason et al[15], and the DFLM structure functions[16], at different $\bar{p}p$ energies. The bands correspond to the uncertainty due to the range in scale, μ, and the range in Λ_5 (which is Λ for 5 active flavors). The $W \rightarrow t\bar{b}$ cross sections are also shown.

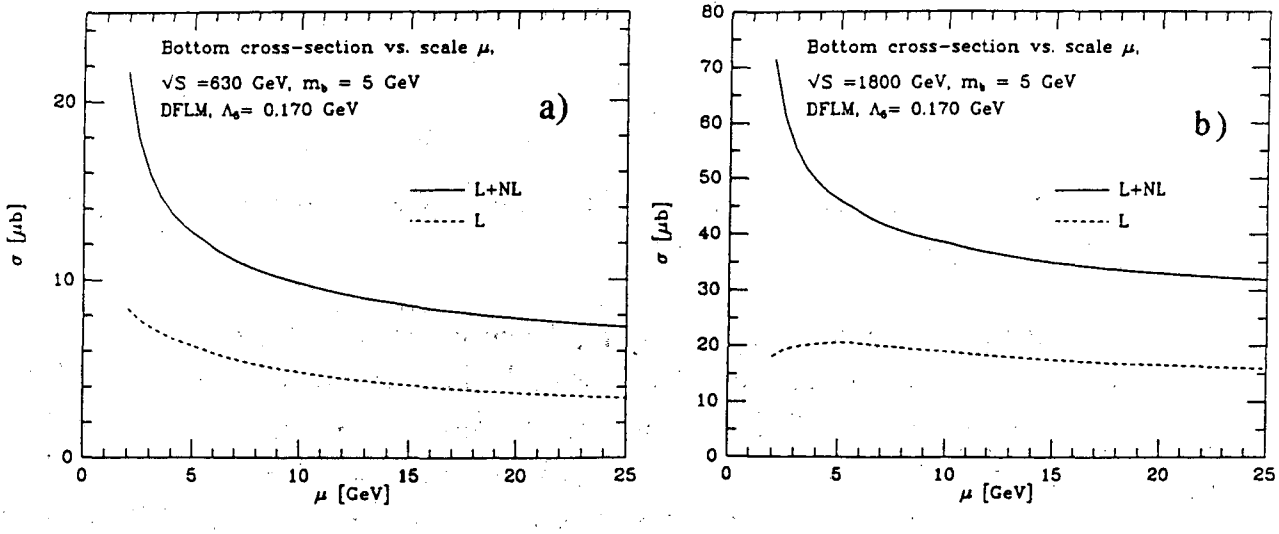

Fig. 5: The total cross section for b pair production (a) at Sp$\bar{p}$S, and (b) at the Tevatron collider energies, as a function of the scale,μ. Dashed lines are for leading order calculations, full lines include the contributions of leading and next-to-leading order.

3. Top Search at HERA

The design parameters of the electron-proton collider HERA, which is in construction at the DESY Laboratory in Hamburg, are listed in Table 1. First collisions are scheduled for 1990.

Table 1. Design parameters of the electron-proton collider HERA.

Electron Energy	30 GeV
Proton Energy	820 GeV
$\sqrt{s}$	314 GeV
Luminosity	$2 \cdot 10^{31}$ cm^{-2}sec

Measurable rates for top quark production are expected for the Bethe-Heitler type of diagrams sketched in Figs. 6b and c. The lowest order process $e^- + \bar{d} \rightarrow \nu_e + \bar{t}$ of Fig. 6a is not expected to contribute significantly since it involves a $\bar{d} \rightarrow \bar{t}$ transition which, within the Standard Model, is predicted to be strongly hindered. The further disadvantage that a $\bar{d}$ sea quark is involved,can be overcome by colliding positrons instead of electrons.

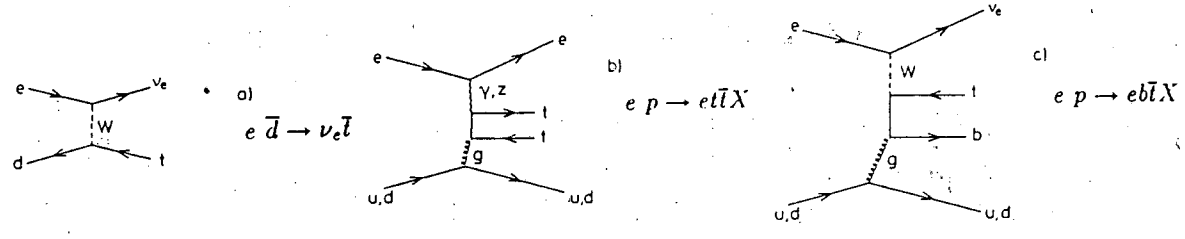

Fig. 6: Diagrams for top quark production. The lowest order diagram a) is not expected to contribute since it involves a d → t transition.

The inclusive t-quark production cross section expected from the boson-gluon fusion diagrams b) and c) in Fig. 1 has been calculated to order $\alpha^2\alpha_s$ by Schuler.[19] Fig. 7, which is taken from Ref.20, shows the various cross section contributions as a function of the top mass, m_t. For $m_t > 55$ GeV the W - g fusion process, $e^- + p \rightarrow \bar{t} + b + X$, dominates over the γ - g fusion, $e^- + p \rightarrow t + \bar{t} + X$, because of the larger phase space available. The contributions of the Z - g fusion as well as of the γ - Z interference term are negligible. The uncertainties of the cross section, which are

mainly due to incomplete knowledge of the gluon structure function, are estimated to be $\leq 30\%$.

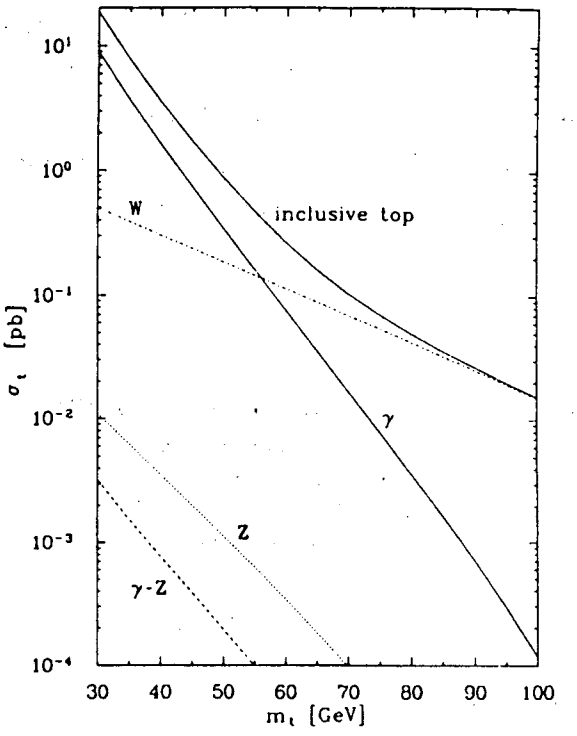

Fig. 7. Cross section for top production via boson gluon fusion, diagrams b) and c) of Fig. 6, at $\sqrt{s} = 314$ GeV. The contributions from W, Z and γ as well as the γ - Z interference term are separately shown.

For $m_t = 70$ GeV and an integrated luminosity of 100 pb^{-1}, an amount one expects to accumulate within a year, about 10 t-quarks are produced. Will one be able to detect these events within a "background" 10^7 times as intense?

This question has recently been studied by Eichler and Kunszt[21] and especially by Ingelman, Schuler and de Trocóniz[22]. Both investigations are quite detailed in the event and background generation. In Ref. 21 emission of an additional gluon in electron scattering of the proton constituents and especially in the diagrams of Fig. 6 for all possible quark combinations is taken into account, but fragmentation effects are treated only globally. In Ref. 22 higher order QCD effects are approximated by using parton shower fragmentation schemes. In both cases, however, the effects of the detector resolution, apart from geometrical acceptance cuts, are not taken into account.

Both investigations conclude that the background becomes negligible by requiring an isolated lepton, which of course has to be not an electron, with large $P_\perp$, a large hadronic transverse energy $\sum E_\perp$, and a large transverse missing momentum, $\not{P}_\perp$. In Fig. 8, which is taken from Ref. 22, the t-quark cross section and the remaining background are shown as function of $\sum E_\perp$, if, apart from an isolated lepton, a $\not{P}_\perp > 10$ GeV is required. A typical isolation requirement is an hadronic energy of less than 1 GeV within a cone of half "angle" $\sqrt{(\Delta\eta)^2 + (\Delta\phi)^2} = 0.4$, where $\Delta\eta$ and $\Delta\phi$ are the distance to the lepton in the laboratory pseudorapidity and

azimuthal angle. The only remaining background is from $b\bar{b}$ production and is negligible for $\sum E_\perp > 40$ GeV. The cut in $\not{P}_\perp$ is certainly problematic because of the detector resolution. But also without such a cut, the background can be separated as is demonstrated in Fig. 9 taken from Ref. 21. Here the cross section for the production of an isolated muon is shown as a function of the $P_\perp$ of the muon for events with 3 or more jets. With such selection criteria the detection efficiency for t-production, including branching ratios, is about 10%.

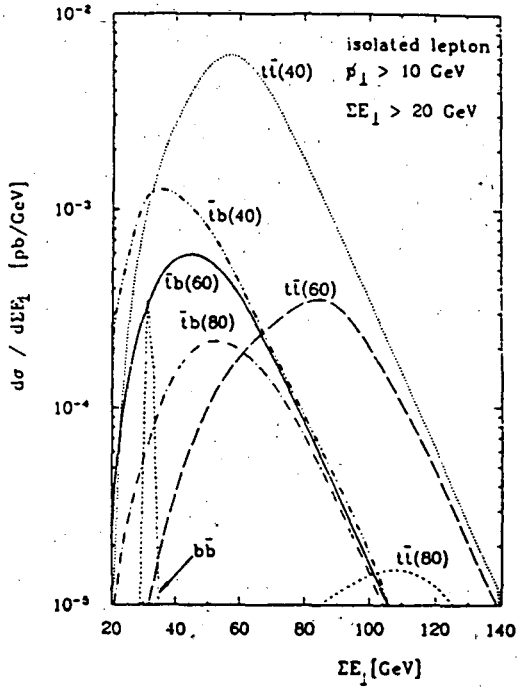

Fig. 8. Differential cross section $d\sigma/d\sum E_t$ versus the total transverse energy, for background and top signal, for three different top masses at $\sqrt{s}$ = 314 GeV (Ref.22). The cuts applied are given in the figure.

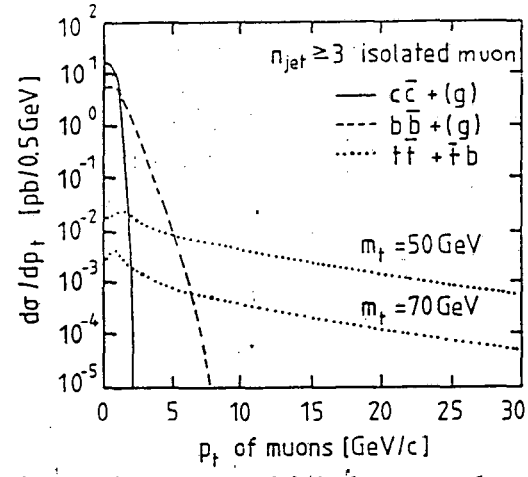

Fig.9. Transverse energy distribution of single muon events for the background and t production for two different t quark masses at $\sqrt{s}$ = 314 GeV (Ref. 21).

A possible background of isolated high $P_\perp$ leptons, which has not been considered in Refs. 21, 22 is from W production $e^- p \rightarrow e^- W^\pm X$ and $e^- p \rightarrow \nu_e W^- X$. The inclusive cross section for W production[23] is about 1 pb at $\sqrt{s}$ = 314 GeV. The two b-quarks, created in the $(\bar{t}b)$-production and the $\bar{t} \rightarrow \bar{b}$ "W" -decay, which are not there in the case of W-production, are probably sufficient to discriminate between W- and t-production. A detailed study is needed, however, since for large m_t both b-quarks tend to be soft and often do not lead to jets.

In summary, one should be able to detect t-production at HERA if $m_t \leq 80$ GeV.

4. Searching for the Top Quark at the Z°Machines

Searches for the top quark at the SLC and LEP utilize the decay mode $Z^\circ \rightarrow t\bar{t}$. However, there is not much phase space left for such searches since we have an unambiguous limit from TRISTAN of $m_t > 27.5$ GeV and a somewhat less direct limit from UA1 of $m_t < 41$ GeV. If indeed there are only three generations, the standard model is pushing us in the direction of higher top quark masses; certainly $m_t < m_{Z^\circ}/2$ is hard to accommodate in the three generation standard model. Nonetheless unambiguous experimental measurements are the final arbiter and hence the experiments at SLC and LEP will certainly search for the top quark. Indeed, if nature is kind and $m_t < m_z/2$, a relatively small data set of several thousand Z°'s will provide a clean signal.

Running at the Z°, the production is totally dominated by the process $Z^\circ \rightarrow t\bar{t}$ for which the cross section is:

$$\sigma(Z^\circ \rightarrow t\bar{t}) = \frac{G_F^2 m_z^4}{8\pi\Gamma_z^2} \{\beta_t (3-\beta_t^2)(1-8/3\sin^2\theta_w)^2 + \beta_t^2\}$$

$$\cong 4\beta_t\{0.075(3-\beta_t^2) + \beta_t^2\} \text{ nb}$$

where G_F is the Fermi coupling, m_z and Γ_z the mass and width of the Z, β_t the top quark velocity and θ_w the weak mixing angle. This cross section can be contrasted with the total hadronic production for 5 quarks (u, d, c, s & b)

$$\sigma(Z^\circ \rightarrow 5 \text{ quarks}) = 27\text{nb}.$$

where we have assumed $m_z = 93$ GeV, $\sin^2\theta_w = 0.23$ and QED radiative corrections have been applied. The production of $t\bar{t}$ is enhanced relative to the formula above by QCD radiative corrections. These corrections tend to be largest as one approaches the threshold of $m_t = m_z/2$. Table 2 summarizes the expected $Z^\circ \rightarrow t\bar{t}$ production rates including the assumed QCD radiative corrections according to Ref.24. One sees that significant production of $t\bar{t}$ persists all the way to the cutoff threshold of $m_z/2$.

Table 2: $Z^\circ \rightarrow t\bar{t}$ production rates for $m_Z = 93$ GeV, $\sin^2\theta_W = 0.23$ including both QED and QCD[24] radiative corrections.

m_t GeV	Branching Fraction ($Z^\circ \rightarrow t\bar{t}$) %	# $t\bar{t}/10^4$ udscb (Produced)
40	3.7	512
42.5	2.7	372
45	1.7	240
46	1.4	195

We assume that the t quark decays via the conventional weak interaction: $t \rightarrow Wb$, where the W is virtual for $m_t < m_W + m_b$.

Certainly one of the first measurements to be made at the SLC/LEP will be the Z° width. One might ask whether this will provide information about $t\bar{t}$ production. For $m_t \geq 40$ GeV, the increase in the Z width is rather small, $\Delta\Gamma_Z \leq 60$ MeV, and even if one did have sufficient sensitivity to see this in the early scans, without direct topological confirmation one would not know what was responsible for the enhanced width. Topological searches are therefore the way to proceed.

There are several topological search procedures which have been studied. The most detailed studies have been performed by the MARKII group and all the results quoted here are from their workshop reports.[25] For these studies, raw data has been generated for full detector reconstruction and therefore the search efficiencies should be considered realistic. For the LEP detectors these efficiencies will be somewhat higher, but the conclusions gained from the MARKII studies are directly applicable to LEP.

The topological search procedures rely on the fact that the t quark is necessarily much heavier than the five known quarks. Clearly the background for the $Z^\circ \rightarrow t\bar{t}$ searches comes from the hadronic decays of the Z° into the five light quarks and more specifically from events which contain gluon radiation. These events can simulate the "fatter" $Z^\circ \rightarrow t\bar{t}$ kinematics. Two search methods are presented here: the use of event shape parameters as an example of a poor technique and isolated leptons as an example of the search method of choice.

The reason that event shape parameters are "dangerous" is that they are subject to our lack of understanding of the fragmentation process. Different Monte Carlo models, all tuned to adequately fit the PEP/PETRA data, do not provide reliable or

consistent background predictions in the kinematic region (multi-jet events) of interest to these searches. The variable most useful for isolating $Z^\circ \rightarrow t\bar{t}$ is the aplanarity as defined in the sphericity tensor scheme.[26] Aplanarity is a measure of the amount of momentum "out of" the event plane. Two-jet events from light quarks have very small aplanarity. However, light quark events can have large aplanarities due to gluon radiation, which result in multi-jet events. For the $Z^\circ \rightarrow t\bar{t}$ one naturally expects large aplanarities because of the heavy t quark mass.

Table 3 summarizes the results of an analysis based on the use of aplanarity. For this simulation 10^4 events of the type $Z^\circ \rightarrow$ hadrons via the 5 known quarks were produced using three different QCD/fragmentation models and the events were reconstructed in the detector. A sphericity analysis was performed on the event and events were excluded if the aplanarity was less than 0.12. The number of (background) events passing this cut are given in the first section of Table 3. The problem alluded to above is now rather clear, namely the background estimates of the different Monte Carlo models vary by a large amount, especially when compared with the expected signal yields, also given in Table 3, for different t quark mass assumptions. The number of $Z^\circ \rightarrow t\bar{t}$ events is normalized to the 10^4 Z° hadronic events using the branching fractions in Table 2, with m_z assumed to be 93 GeV. One might argue that with enough hadronic Z decays, the Monte Carlos could be optimized to give a proper description of the data. However, this cannot be done until one has a complete understanding of all the possible sources of hadrons.

Table 3: The search for top using the shape parameter aplanarity. The first three rows summarize the contributions from the background for three different Monte Carlo models. Note the large variation in the predictions of the different models. The rest of the rows are the signal assuming different top masses.

m_t	# of Events Produced	# of Events with Aplanarity >0.12
Background: Lund $0(\alpha^2_s)$	10^4 udscb	10 ± 3.5
Lund Leading Log	($1.4 \times 10^4 Z^\circ$)	37 ± 5.6
Webber Shower		76 ± 9.0
40 GeV	512	112
42.5 GeV	372	82
45 GeV	240	40

In summary then, the method of shape parameters is a poor way to proceed. This statement is not just true for the aplanarity - all the potentially useful shape parameters suffer the same fate.

The use of large transverse momentum leptons from leptonic decays, does not suffer from the uncertainties of fragmentation and is a clean, high efficiency method of finding top at the Z°. The signal topology involves tagging isolated electrons and muons coming from the decay sequence $Z^\circ \rightarrow t\bar{t}$; $t \rightarrow b + e(\text{or } \mu) + \nu, \bar{t} \rightarrow$ hadron jets. Because of the large t quark mass, the resulting high momentum e and μ are often well isolated from the hadronic jets.

The background comes potentially from $Z^\circ \rightarrow b\bar{b}$; $b \rightarrow c + e(\text{or } \mu) + \nu$, $\bar{b} \rightarrow$ hadron jets. However, in this case even when the e or μ have high momentum, they are not isolated from the hadronic jets.

A clean separation of the signal is obtained with relatively simple cuts which have good efficiency. Multiparticle events are selected which have a lepton (electron or muon) with transverse momentum ($P_\perp$) relative to the thrust axis larger than 3 GeV/c. The hadrons are then partitioned into jets using a cluster algorithm. The lepton isolation parameter is then calculated for each jet (j) as follows:

$$\rho_j = \{E_\ell(1 - \cos\theta_{\ell j})\}^{1/2}$$

where E_ℓ is the lepton momentum and $\theta_{\ell j}$ is the angle between the lepton and the axis of the jth jet: ρ_j^2 is effectively the invariant mass of the lepton-jet system assuming the jet mass to be 1 GeV. The lepton isolation parameter for the event is chosen as

$$\rho = \min\{\rho_j\}.$$

Figure 10 shows $dn/d\rho$ for a background sample of 10^4 Z°'s decaying to the five light quarks and for a sample of appropriately normalized $Z \rightarrow t\bar{t}$ events (see Table 2), $m_t = 40$ GeV. Both electrons and muons are used in this analysis and both the signal and background are subject to the selection criteria given above. A cut at $\rho > 1.8$ GeV$^{1/2}$ provides an efficient and clean $Z^\circ \rightarrow t\bar{t}$ signal. Predictions of the background spectrum have been verified to be independent of the QCD/fragmentation model as indicated in Table 4 which summarizes the sensitivity of the selection technique for different t quark masses. Again, $m_Z = 93$ GeV was assumed for these simulations.

The isolated lepton search procedure for $Z^\circ \rightarrow t\bar{t}$ is robust and particularly free of background. The efficiency is high enough that with 1000 Z° events one would have a significant excess of events for $m_t \leq 43$ GeV, with 5000 events one could explore the region very close to the kinematic threshold of $m_Z/2$. With 50,000

events one could begin a rather thorough study of the properties of the $Z^\circ \rightarrow t\bar{t}$ decays using this clean, unbiased sample.

Table 4: The search for top using the isolation criteria described in the text. The first two rows summarize the contribution from the background for two different Monte Carlo models. The rest of the rows are the signal assuming different top masses. As described in the test, $\rho > 1.8$ GeV$^{1/2}$ and $P_\perp > 3$ GeV/c are the primary analysis cuts for the isolated lepton.

	# of Events Produced	# of Isolated Lepton Events	Signal: Background
Background: Lund Leading Log Webber	10,000 udscb ($1.4 \times 10^4 Z^\circ$'s)	2.6 ± 1.5 3.3 ± 1.9	
$m_t = 40$ GeV Lund Symmetric Webber	512	76 ± 2.2 74 ± 4.3	25:1
$m_t = 42.5$ GeV Lund Symmetric Lund Peterson	372	61 ± 4.7 62 ± 1.5	20:1
$m_t = 45$ GeV	240	38 ± 3.1	13:1
$m_t = 46$ GeV	195	30 ± 2.4	10:1

Clearly the technique described for the t quark search is rather general - it will isolate events coming from all strongly coupled objects which are produced in pairs in Z decays. In particular the method will isolate events of the type $Z^\circ \rightarrow b'\bar{b}'$,where the b' is a 4th generation, charge -1/3 quark. The issue thus becomes: could one distinguish these two sources - is it a t or b'?

In the absence of a good measurement of the quark mass, and reliable QCD radiative corrections to the production cross section, using the absolute rate will not be useful. However, if we assume that $m_{b'} < m_t$, which is a safe assumption for this scenario, b' decays are distinguishable from t decays because they result in a lot of leading charm (D*'s) which is not true for t decays:

$$b' \rightarrow c + W \qquad\qquad t \rightarrow b + W$$

The b from the t will decay to charm, but these charm jets will not produce leading D*'s. So the trick for distinguishing b' jets from t jets is to tag $D^{*\pm}$'s which carry a large fraction of the beam energy. D*'s can be tagged using the famous ΔM technique[27], but this method has a very low efficiency since specific low branching

fraction modes of the D° enter. As discussed in Ref. 28, an inclusive D* tag is possible if one recalls that the bachelor pion in the decay $D^{*\pm} \rightarrow \pi^{\pm} D^{\circ}$ has very little momentum transverse to the D* flight direction ($\langle P_{\perp} \rangle \sim 30$ MeV/c). This can be contrasted with the typical fragmentation pion which has $\langle P_{\perp} \rangle$ of 300 MeV/c. We use this low $P_{\perp}$ as an inclusive tag for charm.

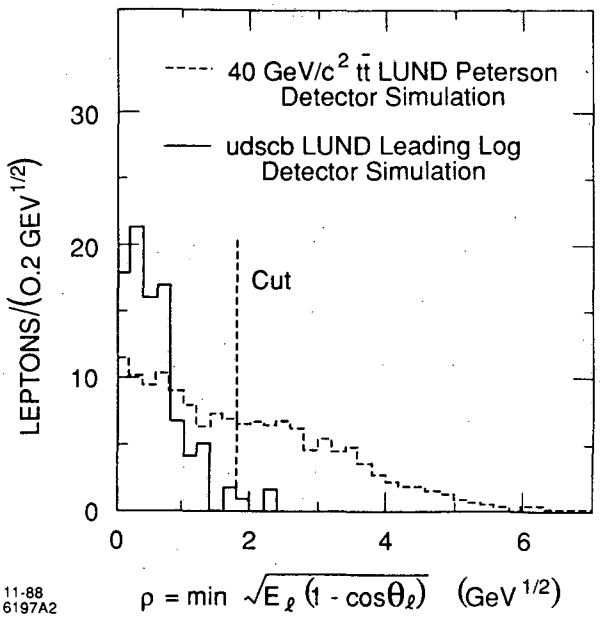

Fig. 10: Isolation criterion for leptons with $P_{\perp} > 3$ GeV/c. Distribution of ρ (defined in text) for leptons with $P_{\perp} > 3$ GeV/c for 10,000 *udscb* events from the Lund leading-log model with full detector simulation and for 512 $t\bar{t}$ events with $m_t = 40$ GeV from the Lund model with Peterson fragmentation.

In order to make this tag useful for separating t and b', one must remove contamination coming from $Z \rightarrow b\bar{b}, c\bar{c}$. This can be done by making a series of cuts which favor the heavy quark events and discriminate against slow D*'s; the full details can be found in Ref.28. Multihadronic events are partitioned into jets using a cluster algorithm. Events with the event thrust > 0.9 are rejected. This cut favors the heavy quark events and discriminates strongly against $Z^{\circ} \rightarrow c\bar{c}$. Each charged track's $P_{\perp}$ is measured relative to the axis of the jet to which it belongs. A further cut is made for candidate bachelor pions requiring them to have $z = E^{\pi}/E_{cluster}$ between 0.04 and 0.08 where E^{π} and $E_{cluster}$ are the charged particle and cluster energy, respectively. This requirement discriminates against D* produced in b quark decays in which the bachelor pions are softer than these cuts permit. Figure 11a shows the $P_{\perp}^2$ spectrum for charged particles in a sample of 500 events of the type $Z \rightarrow b'\bar{b}'$ ($m_{b'} = 45$ GeV). The events and charged particle candidates satisfy the criteria discussed above. One sees the clear excess of low $P_{\perp}$ tracks coming from the D*'s superimposed on the typical fragmentation spectrum with slope ~ 300 MeV/c. Figure 11b shows the same distribution for a sample of $Z \rightarrow t\bar{t}$ events ($m_t = 45$ GeV) for

which no hard D* component can be seen. Finally, Figure 11c shows the $P_\perp{}^2$ distribution for a sample of 10^4 decays of Z° to the five light quarks plus 500 Z° → b'b̄' and Z → tt̄ scenario. Thus these two scenarios are distinguishable. It is worth noting that this inclusive method is about 10 times more efficient than the more standard ΔM method. In the data set of 500 b'b̄' events, 125 tagged $D^{*\pm}$ are found (Fig. 11a). Applying the ΔM method and using as many D° decay modes as possible one finds 12 exclusively tagged events.

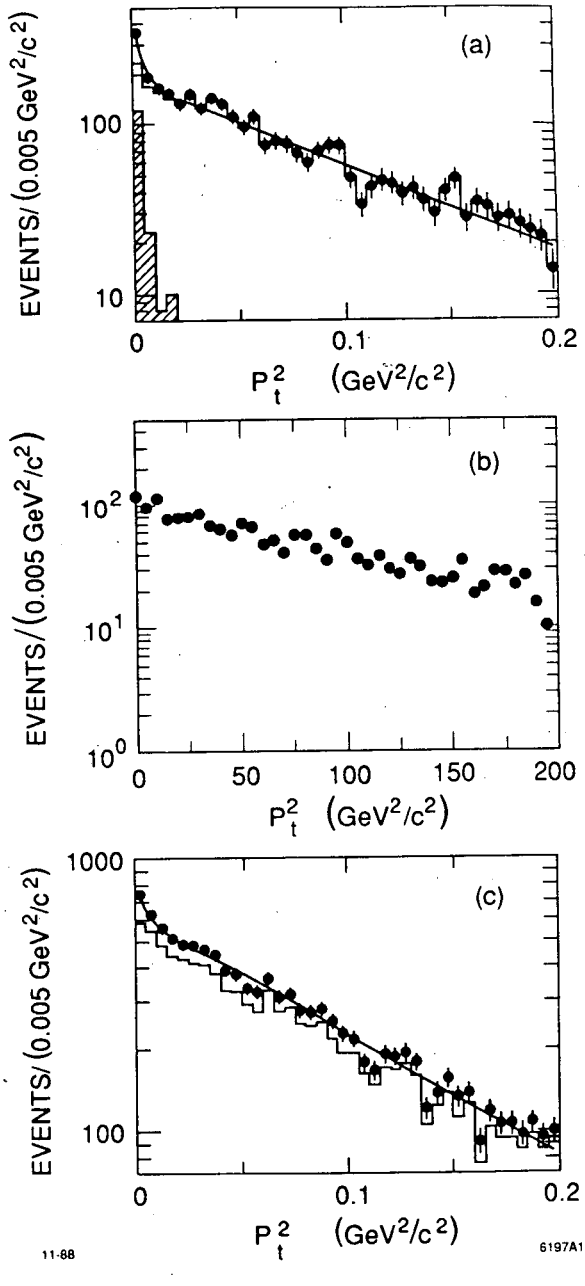

Fig. 11a: $P_\perp{}^2$ distribution for bachelor candidates (data points) obtained in the decay of a 45 GeV b' quark. The solid histogram corresponds to candidates not coming from a D* and the hatched histogram to candidates coming from a D*. The solid line is a fit to the data with two Gaussians, one of slope ~ 30 MeV/c, the other ~ 300 MeV/c.

Fig. 11b: The sames as 2a except for a sample of $Z^o \rightarrow t\bar{t}$ with $m_t = 45$ GeV.

Fig. 11c: $P_\perp{}^2$ distribution for bachelor candidates (data points) obtained in 10,000 Z^o decays containing 500 b'b̄' events. The histogram corresponds to only normal Z^o decays (*udscb*). The solid line corresponds to the fit of two Gaussians to the total sample.

There are several possible ways to measure m_t once one has a signal. These include counting the yield of high $P_\perp$ leptons, fitting the shape of the $P_\perp$ distribution, reconstructing the hadronic jet mass in the isolated lepton events...All these methods suffer from one deficiency or another and yield typical mass uncertainties of about 2 GeV for the mass range and event sample sizes (~ 10^4Z's) discussed here. Presumably if a precise measurement of m_t was needed, one could lower the beam energy and scan for toponium using the crude measurement as a guide. This will require a relatively large luminosity ($\approx 10^{30}cm^{-2}sec^{-1}$) to find toponium in a reasonable time. In addition, if the toponium mass is very close to $m_Z/2$, interference effects greatly distort the toponium shape and make it impossible to find[25].

In conclusion, the Z° resonance is an excellent place to search for top as long as it is sufficiently low in mass to be produced. With 10,000 Z° events one would have sensitivity to masses up to $m_Z/2$. The possible confusion between a top quark and a b' quark is easily resolved. Mass estimates in the range of ± 2 GeV are possible.

5. Finding the Top at Lep II

5.1 A comment on the upper limit $m_t < 200$ GeV

All we know at present of the top mass is that it is very likely to exist and that its mass is in the range $41\ GeV \leq m_t \leq 200\ GeV$.

The non-existence of the top mass would be extremely delicate to accommodate theoretically. The lower limit on its mass comes from its non-observation in $p\bar{p}$ collider experiments[6,7]. The upper limit comes from neutral-current phenomenology[14,29].

It should be emphasized, however, that this upper limit is valid within the strictly minimal Standard Model only: a deviation of the tree-level ρ_{tree} parameter from 1 and a very heavy top-quark mass would produce the same effects on m_w, m_z, and $\sin^2\theta_w$. For instance,[30] the combination of $m_t = 330$ GeV and $\rho_{tree} = 0.96$ would not be distinguishable by electroweak measurements from $m_t = 45$ GeV, $\rho_{tree} = 1$. A value of ρ_{tree} slightly different from 1 can be generated if there exist triplets of Higgs with non-vanishing vacuum expectation values. Such accidental cancellation seems unnatural but cannot be excluded.

5.2 Finding the top at LEP II

Of course neutral-current phenomenology will receive a considerable boost when detailed studies of the Z resonance become available at LEP. The basic degeneracy between m_t and ρ will, however, remain. The uncertainty on the top mass certainly obscures the interpretation of precision measurements, but it will hopefully be removed by the direct observation of the top at LEP II.

After a first phase of running at and around the Z peak, LEP will be equipped progressively with superconducting RF cavities to reach a maximum energy of E_{beam} = 95 GeV per beam[31]. The expected event rates for the dominant processes are shown in Fig.12. Two features dominate LEP II physics: i) the dominance of the radiative tail of the Z over rather small point-like cross-sections, and ii) the occurrence of the W-pair threshold. Both will make finding the top somewhat less straightforward at LEP II than in lower energy machines.

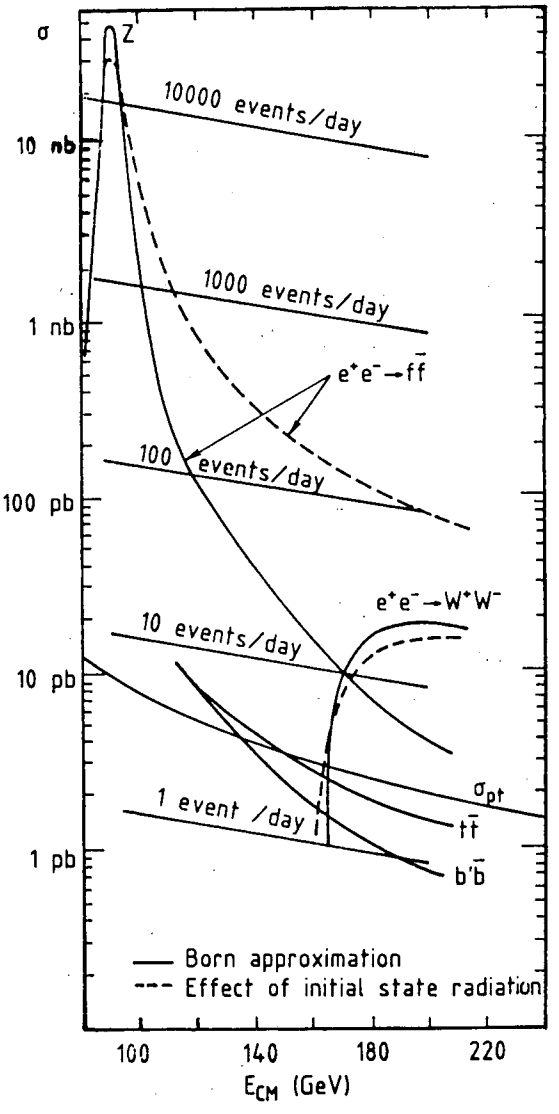

Fig.12: Cross-sections and rates in the energy range of LEP II. For heavy flavour production, the $t\bar{t}$ and $b\bar{b}'$ cross section 10 GeV above threshold is indicated.

The procedure to discover the top at LEP II is described in Ref. 32 and will be briefly summarized here. Two cases have been distinguished:

a) $m_t < m_W$

b) $m_t > m_W + m_b$

The intermediate situation, $m_t \in [m_W, m_W + m_b]$ has not yet been investigated in detail.

In case (a) the first thing to do is to remove the Z radiative tail by applying a cut on the missing longitudinal momentum (Fig. 13a). The plot was made for a b' with mass $m_{b'} = 65$ GeV, but it would be the same for a top with the same mass. Sphericity and aplanarity distributions can then be used to enhance the new quark production (Fig.13b). For the light quarks these distributions can be accurately calibrated beforehand with high statistics Z-peak data. The cross section within these cuts exhibits a threshold effect (Fig.13c). An integrated luminosity of 15 pb^{-1} has been estimated necessary to find a new b' if $m_t < m_{b'}$ or even less to find the top, or a new b', if $m_{b'} < m_t$.

In case (b) ($m_t > m_W + m_b$), the top-production threshold has to be distinguished from the W-pair threshold. If the heavy quark produced is a b', and the top is lighter, then $b' \rightarrow Wt$, where the W is virtual.One can purify a b' signal by first eliminating WW events with one or more semileptonic decays, $W \rightarrow \ell\nu$. For the rest, WW events are expected to have less charged tracks and a distribution of jet-jet masses peaked around m_W (Fig.14a). In the case of top production, life is even harder since the dominant top decay is $t \rightarrow bW$, where the W is real, resulting in events very similar to W pairs, because the b is soft. One nice way out of this difficulty is to reconstruct the W direction; top-induced W's are isotropically produced, in contrast with direct WW production, peaked at small angle with W's emitted back-to-back (Fig.14b).

WW events are expected to have less charged tracks and a distribution of jet-jet masses peaked around m_W (Fig. 14a). In the case of top production, life is even harder since the dominant top decay is $t \rightarrow bW$, where the W is real, resulting in events very similar to W pairs, because the b is soft. One nice way out of this difficulty is to reconstruct the W direction; top-induced W's are isotropically produced, in contrast with direct WW production, peaked at small angle with W's emitted back-to-back (Fig. 14b).

The resulting threshold is visible (Fig.14c) but requires more data (50 pb^{-1}). Case (b) would be somewhat unfortunate since both top and W-pair productions would be made substantially more difficult.

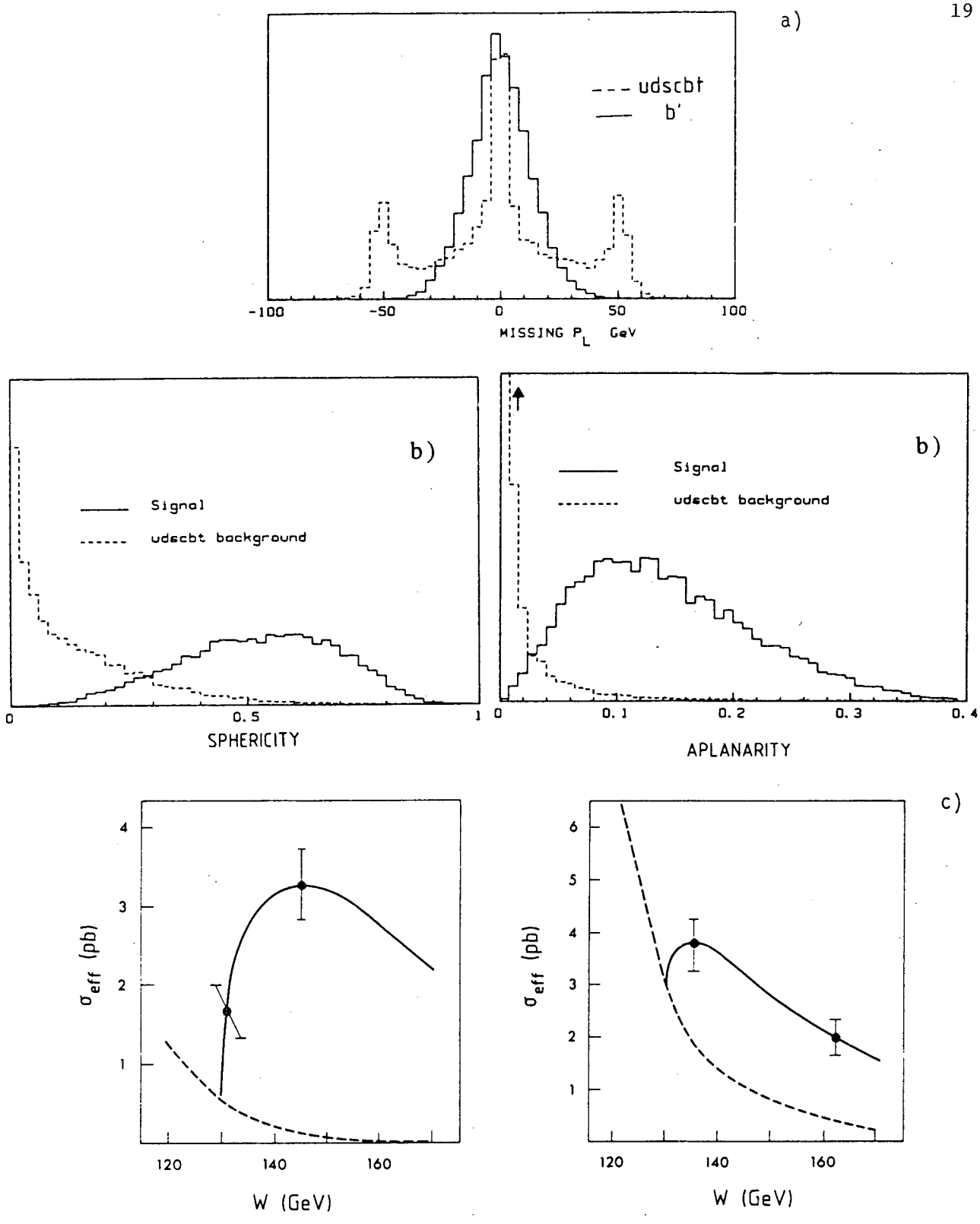

Fig.13: Heavy quark selection, for $m_t \leq m_W$. a) Missing longitudinal momentum for light (udscbt) and heavy (b') quarks. $m_t = 45$ GeV, $m_{b'} = 65$ GeV. b) Sphericity and aplanarity distributions for light and heavy quarks, $m_t = 45$ GeV, $m_{b'} = 65$ GeV. c) Effective cross section for $t\bar{t}$ production (full line) and background (dotted line) after missing P_L and aplanarity cut. Error bars are calculated for an integrated luminosity of 15 pb^{-1}. Left: $m_t = 65$ GeV, right: $m_t = 45$ GeV, $m_{b'} = 65$ GeV.

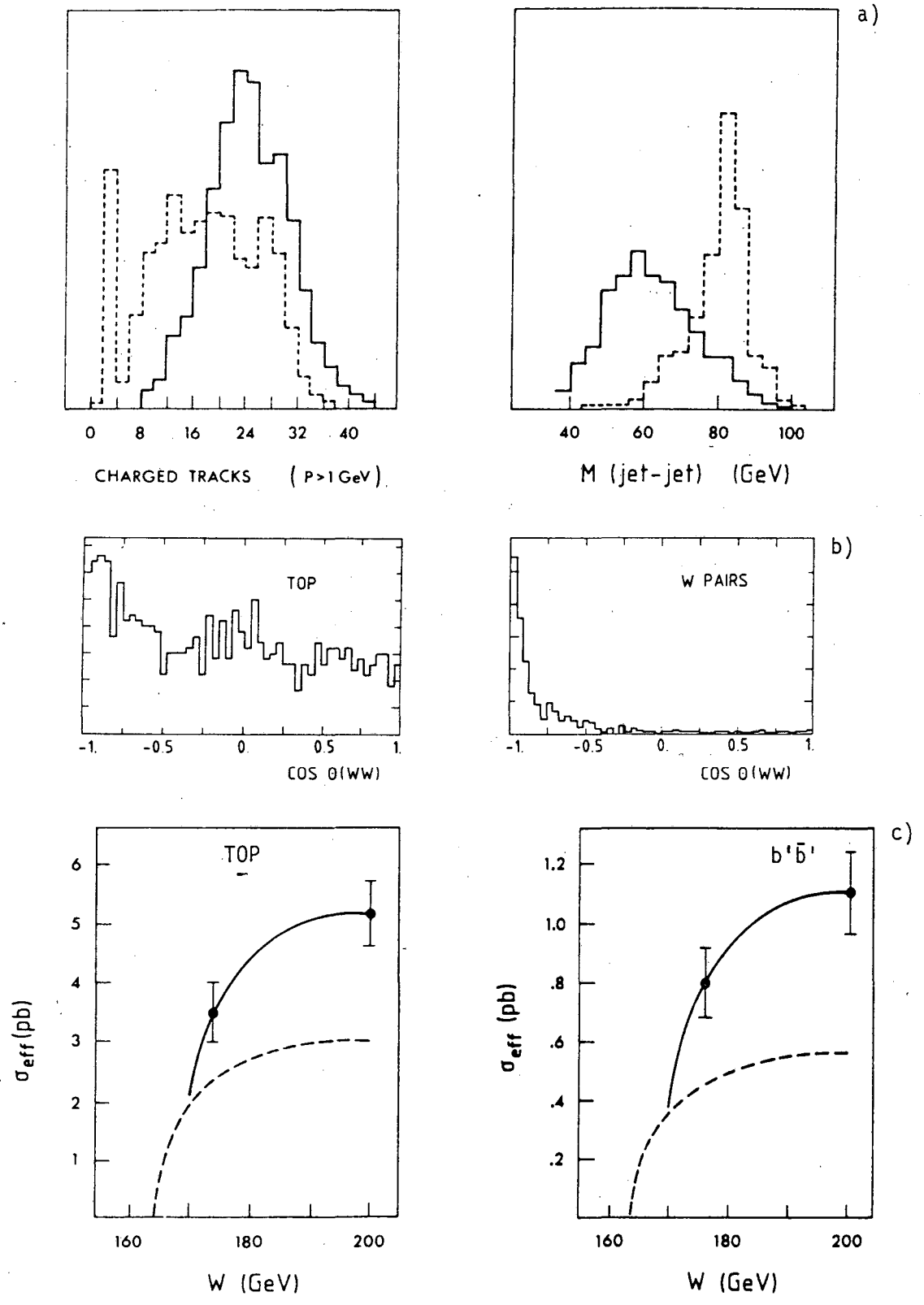

Fig.14: Heavy quark selection, for $m_t > m_W + m_b$. a) Charged track multiplicity and jet-jet invariant mass closest to the W mass for b'b̄' production(full line) and $W^+ W^-$ production (dotted line). b) The angular distribution of the two W's relative to each other, for top $m_t = 85$ GeV and for the WW background. c) Effective cross-section for heavy flavour production (full line) and background (dotted line) after cuts. Error bars are calculated for an integrated luminosity of 50 pb^{-1}. Left: $m_t = 85$ GeV, right: $m_t = 45$ GeV, $m_{b'} = 85$ GeV.

5.3 Study of top and toponium properties

It is very possible that a $p\bar{p}$ collider will have found evidence for the top before the necessary energy is available at LEP. The unique feature of e^+e^- machines is then to offer the possibility of studying the top via its direct and clean production, evaluate its mass precisely, and determine its properties, charge, spin, decay modes, fragmentation function, etc.

Furthermore, the toponium, $t\bar{t}$ bound state $\theta(1s)$, can be found[33], as well as its first radial excited state $\theta(2s)$, at the expense of a larger investment in integrated luminosity. Fig.15 shows the integrated luminosity required to find these bound states from a binary scan, assuming that the top mass is known before hand with a precision of 2 GeV.

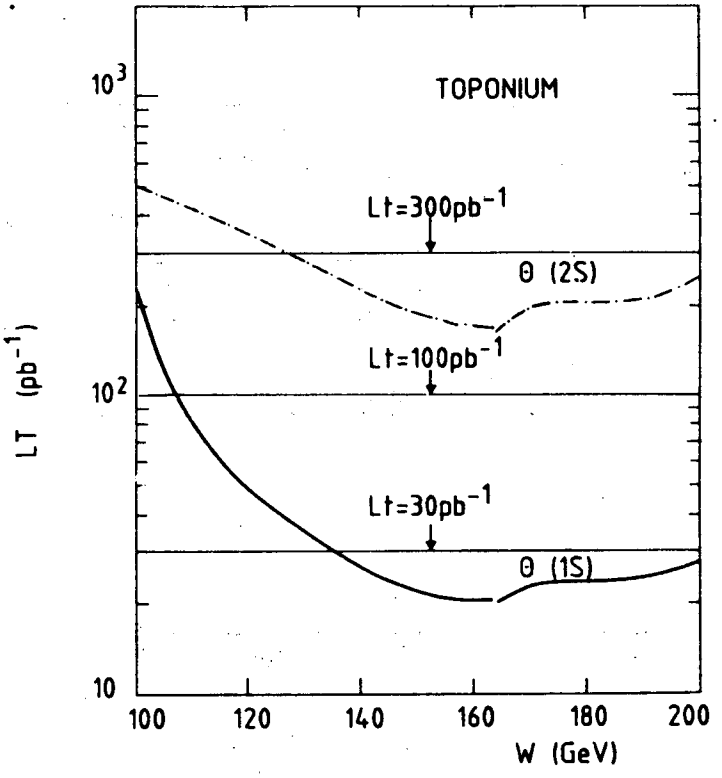

Fig.15: Total luminosity needed to detect toponium (1S and 2S) with a significance of 3 standard deviations.

The toponium is a laboratory for numerous experiments. The $\theta(1s)$ - $\theta(2s)$ mass difference is a clue to the quark-quark potential, presumably predictable by perturbative QCD for such high masses.

Of particular interest is the possibility of finding the Higgs in toponium decay[34], $\theta \rightarrow H\gamma$, for $m_H \leq 0.9\ m_\tau$. The toponium branching fractions and rates are shown in Fig.16a; the $H\gamma$ decay competes with the very abundant direct decay $t \rightarrow$

bW. The effective cross section for Higgs production is therefore reduced rapidly when the toponium mass becomes too heavy, and this method becomes uncompetitive for $m_\theta \geq 120$ GeV.

This difficulty would not occur if the b' were to be discovered, the single quark decay of the b'$\bar{b}$' bound state being presumably suppressed by the generation gap (Fig.16b). The bottomonium (prime) would thus offer the possibility of finding the Higgs for $m_H \leq 0.9\, m_{b\bar{b}} \leq 180$ GeV.

5.4 Summary[35]

The possibilities for finding and studying the top and its bound states are summarized as follows.

a) When?

Beginning year	E_{cm} (GeV)	Maximum mass at which the top will be seen and studied (GeV)
1989-1991	≤ 110	50
1992-1993	≤ 130	60
1994-1995	≤ 160	75
> 1995	≤ 190	90

b) With what required luminosity?

$m_t < 75$ GeV (pb^{-1})	$m_t > 75$ GeV (pb^{-1})	
15	50	Establish the top (5σ) $\Delta m_t \approx \pm 10$ GeV
100	200	Measure threshold, $\Delta m_t \approx \pm 2$ GeV
25	25	Find toponium $\theta(1s)$
200	200	Find 1st excited state $\theta(2s)$

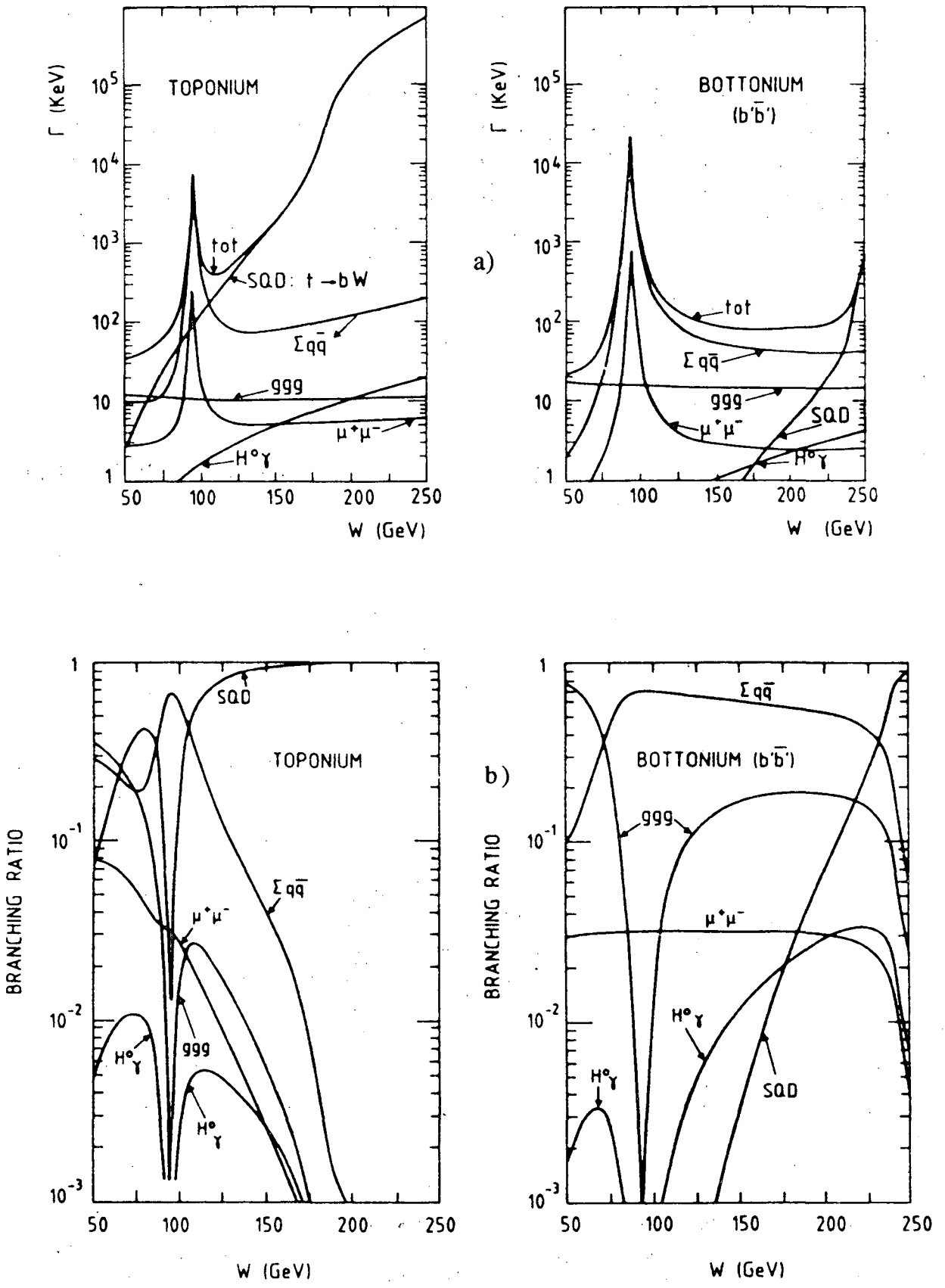

Fig.16: a) Total and partial decay widths for the most prominent toponium and bottomonium (prime) ground-state decays. b) Decay branching ratios for the toponium and bottomonium (prime) ground states.

6. Top Search in UA2'

The main physics goal of the data taking in 1988 and 1989 at the improved CERN SpS̄S Collider is to search for top with a mass m_t above 40 GeV, given the lower limit, $m_t > 41$ GeV (95% CL), measured by UA1[6,7], and the upper limit $m_t < 180$ GeV (90 % CL), deduced in the framework of the Standard Model[14]. At hadron colliders the t-quark is expected to be produced mainly through two mechanisms:

electroweak production $p\bar{p} \rightarrow W + X$ (6.1)

$\hookrightarrow t\bar{b}$

QCD production $\bar{p}p \rightarrow t\bar{t} + X$ (6.2)

where the second mechanism proceeds through gluon fusion and quark annihilation.

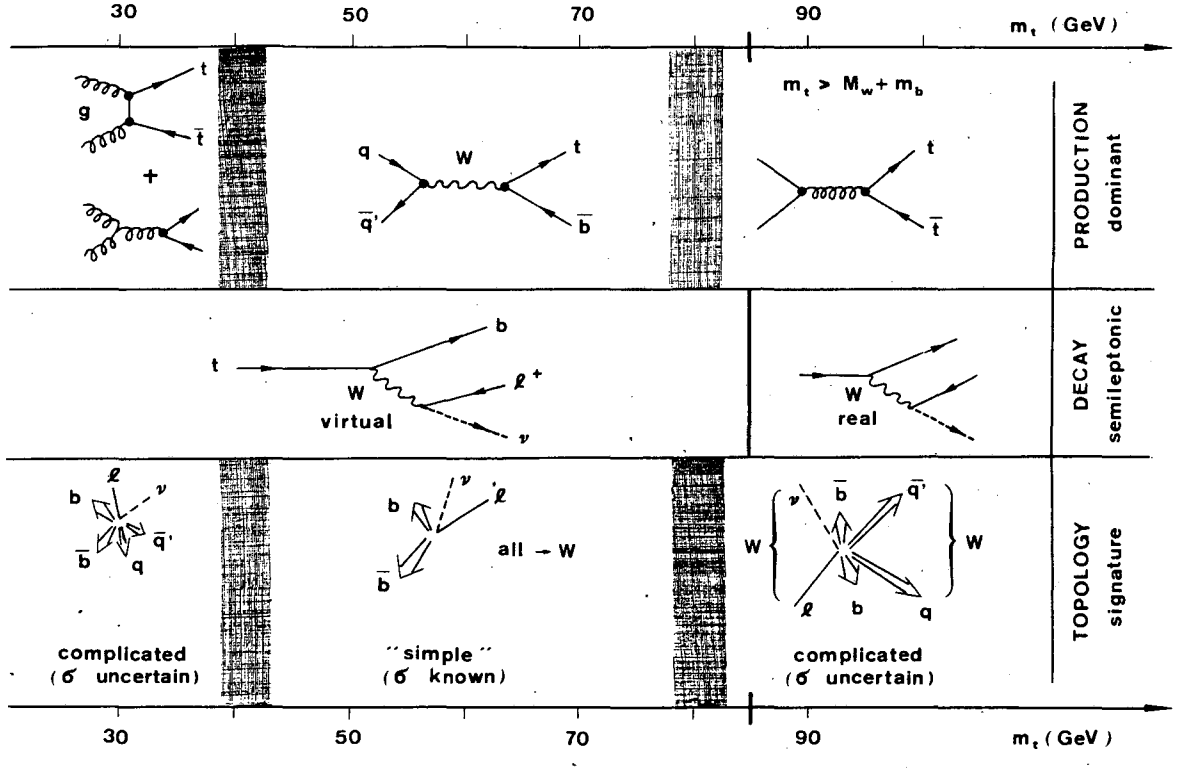

Fig.17: Schematic presentation of top ($t\bar{t}$ and $t\bar{b}$) production and subsequent semileptonic decay at the CERN SpS̄S Collider ($\sqrt{s} = 630$ GeV). The event topology, shown in the plane transverse to the beam axis, implies the following top signature: ℓ(isolated) + ≥ 2 jets (+ $\not{P}_T$), where ℓ means charged lepton (electron in UA2') and $\not{P}_T$ missing transverse momentum due to the undetected neutrino. With increasing heavy quark mass the decay lepton is expected to be more and more isolated.

Figure 17 shows the dominant processes and the corresponding event topologies, in the plane transverse to the beam axis, for $t\bar{t}$ and $t\bar{b}$ production and subsequent semileptonic decay at $\sqrt{s}$ = 630 GeV. The contribution from the electroweak process (1), which dominates the QCD $t\bar{t}$ production (Eq. 6.2) for 40 GeV< $m_t < M_W - m_b$, can be predicted quite accurately as a function of m_t by using the measured cross-section $\sigma(p\bar{p} \rightarrow W \rightarrow e\,\nu)$ and taking into account the known phase-space factor[36]. For higher values of m_t, top is produced by the QCD process (Eq. 6.2), whose cross section calculation is less reliable mainly due to uncertainties in structure functions and in the choice of the Q^2 scale. However,as discussed in Sec. 2.1, a recent next-to-leading order QCD calculation leads to a firmer prediction of heavy-flavour production[15,7]. Because of the large QCD multijet background, UA2' is searching for top by investigating final states containing an isolated electron and two or more jets (see Fig. 17). Taking advantage of the considerably improved electron identification of UA2', as a consequence of the new central detector[37,38], Figure 18 presents the expected number of top events[39] as a function of m_t, with

- one reconstructed isolated electron with $P_\perp{}^e > 12$ GeV and
- at least two reconstructed jets with $P_\perp j_1 > 10$ GeV and $P_\perp j_2 > 8$ GeV

for an integrated luminosity of 10 pb^{-1}. In order to keep the background from fake electrons low, i.e. around 10 events, a set of tight electron cuts are required. At this level the top analysis still suffers from background processes yielding real electrons:

b-quark production	$p\bar{p} \rightarrow b\bar{b}(g)$ $\hookrightarrow c e \nu$
production of W with jets	$p\bar{p} \rightarrow W + 2j + X$ $\hookrightarrow e\nu$

The application of strict isolation criteria to the calorimeter as well as preshower response of the electron candidate helps to reduce the limiting $b\bar{b}$ background, which is, by the way, not easy to predict (cross-section, fragmentation, calorimeter response to low-energy particles).

Summing up all these background levels shown in Fig. 18, we expect more signal than background events for $m_t < 60$ GeV. Since the $P_\perp{}^e$ spectrum for the semileptonic decay $b\bar{b}$ is steeply falling, an increase of the $P_\perp{}^e$ threshold (from 12 to 15 ÷ 20 GeV for $m_t \approx 60$ GeV) should result in a sizable reduction of this background. Furthermore, using topological cuts and invariant mass reconstructions, we anticipate to collect a rather clean top sample for t-quark masses up to 70 GeV for an integrated luminosity of 10 pb^{-1}.

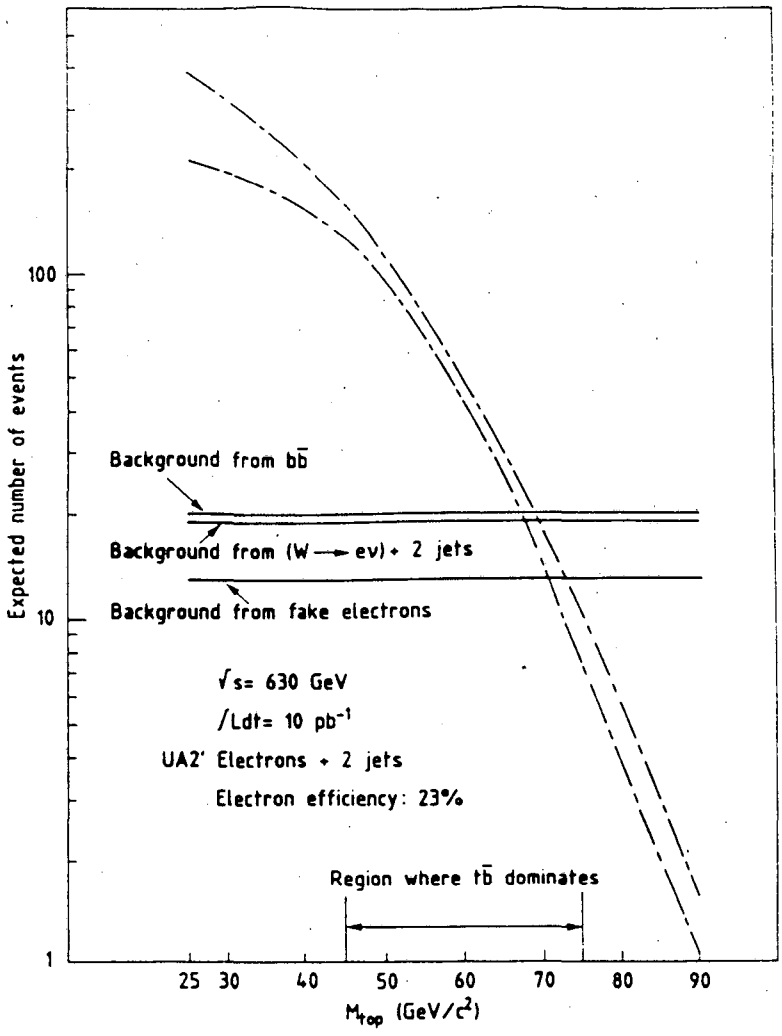

Fig.18: Expected number of reconstructed semileptonic top decays in UA2' ($P_\perp^e > 12$ GeV, $p_\perp j1 > 10$ GeV, $p_\perp j2 > 8$ GeV) for an integrated luminosity of 10 pb^{-1} as a function of the t-quark mass. The range for the number of top events is predicted by Ref. 7. The expected background levels from fake electrons and from real electron sources (semileptonic b-decay, W decay) are also shown. Acceptances and selection efficiencies are taken into account.

7. TOP SEARCH IN UA1

7.1 The present lower limit on M_t from UA1

UA1 has made a systematic search for the top quark in the ~ 0.7 events/pb of data accumulated between 1982 and 1985. The top is searched through its semileptonic decay modes $t \rightarrow b\, e/\mu\nu$, the UA1 apparatus having e and μ detection capability. Fig.19 shows the expected top production rates at $\sqrt{s}$ = 0.63 TeV for experimental sensitivities of 0.7 events/pb, the present one, and of 10 events/pb, which might be expected under favorable conditions by the end of 1989. The event

numbers in Fig.19 take into account only the $t \rightarrow b\, e/\mu\nu$ leptonic branching ratio, but not the detection efficiency, which is of the order of few percent for $m_t \sim 25$ GeV and increases to ~ 35% at $m_t > m_W$. As visible from Fig.19, there are three distinct dynamical regimes for top production and decay at $\sqrt{s} = 0.63$ TeV. For $m_t < 45$ GeV the dominant production mechanism is the QCD production of $t\bar{t}$ pairs, for 45 GeV < $m_t < m_W$ the dominant contribution is through W production followed by a $W \rightarrow t\bar{b}$ decay, while for $m_t > m_W$ only $t\bar{t}$ production remains. The interesting aspect of this latter top mass range is that for $m_t > m_W$ the top decays into $t \rightarrow Wb$ with a physical (on-shell) W, $t\bar{t}$ production thus giving rise to $t\bar{t} \rightarrow WWb\bar{b}$ final states with a rather remarkable $WW \rightarrow (l\nu)$ (jet-jet) final state signature.

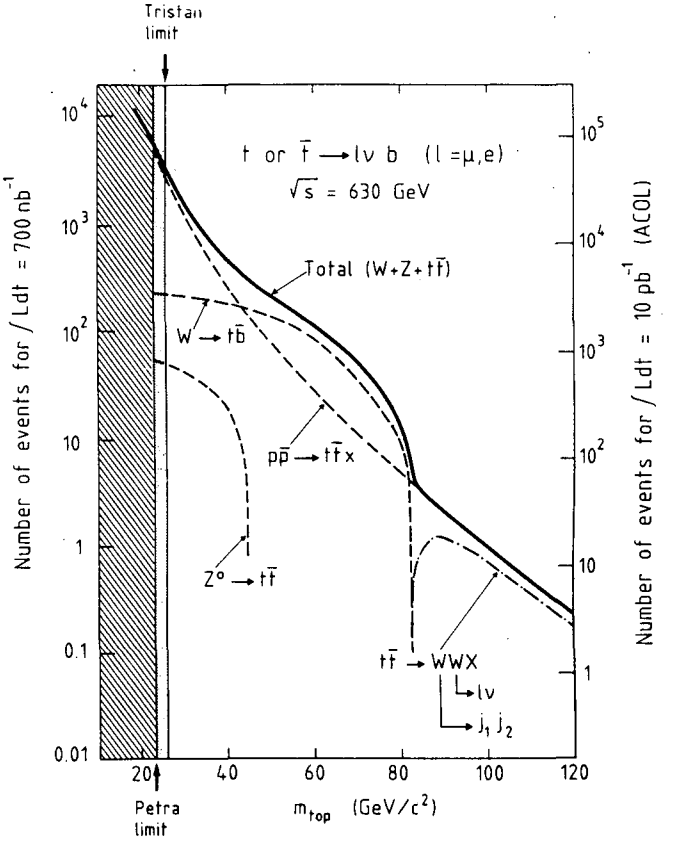

Fig. 19: Expected top production rates at $\sqrt{s}$ = 0.63 TeV for experimental sensitivities of 0.7 and 10 events/pb.

The experimental statistics available until now allowed a systematic investigation of the region $m_t < 45$ GeV. The results of the study of $e/\mu + \geq 1$ jet final state events by UA1[6] are summarized in Fig.20. This study provides no evidence for top in this mass range and gives a lower limit of $m_t > 44$ GeV. In Figure 20 the limit is expressed in terms of a ratio $K = \sigma_{t\bar{t}} / \sigma^{\circ}_{t\bar{t}}$ of some $t\bar{t}$ production cross section, $\sigma_{t\bar{t}}$, to a nominal theoretical $t\bar{t}$ production cross section $\sigma^{\circ}_{t\bar{t}}$. For the latter one we take the lowest order (α_s^2) QCD production cross section using the structure functions EHLQ1 with a scale $Q^2 = m_t^2 + P_\perp^2$. Taking in the numerator of the ratio K for $\sigma_{t\bar{t}}$ the experimental 95% C.L. upper limit on the $t\bar{t}$ production (the possible $t\bar{b}$

contribution has been subtracted from the data), we obtain the curve labelled (a). The intercept of this experimental upper limit (a) with a reasonable theoretical lower limit on $t\bar{t}$ then provides a lower limit on m_t. Fig.20 shows a number of theoretical options for $\sigma_{t\bar{t}}$ (relative to the nominal one) we have investigated. The most conservative QCD expectation for $t\bar{t}$ production was provided by the lowest order $t\bar{t}$ calculation with DO1 structure functions and $Q^2 = \hat{s}^2$, curve (b) in Fig.20. The intercept of the two curves (a) and (b) gives the UA1 lower limit $m_t > 44$ GeV at 95% C.L. In the meantime appeared in the literature the complete (up to order α_s^3) QCD calculation of heavy flavour production by Nason et al.[15], and the new set of structure functions of DFLM[16]. These structure functions are based on the latest deep inelastic neutrino scattering data and have a softer gluon distribution than earlier parameterizations. The reanalysis in Ref.7 of the UA1 experimental upper limit on $t\bar{t}$ in terms of these new theoretical developments yields a slightly more conservative lower bound $m_t > 41$ GeV (Fig.21). In this estimate of the lower theoretical bound on $t\bar{t}$ production α_s^3 terms are now included, but also uncertainties on α_s (i.e. Λ_{QCD}), the Q^2 scale and DFLM structure functions are employed.

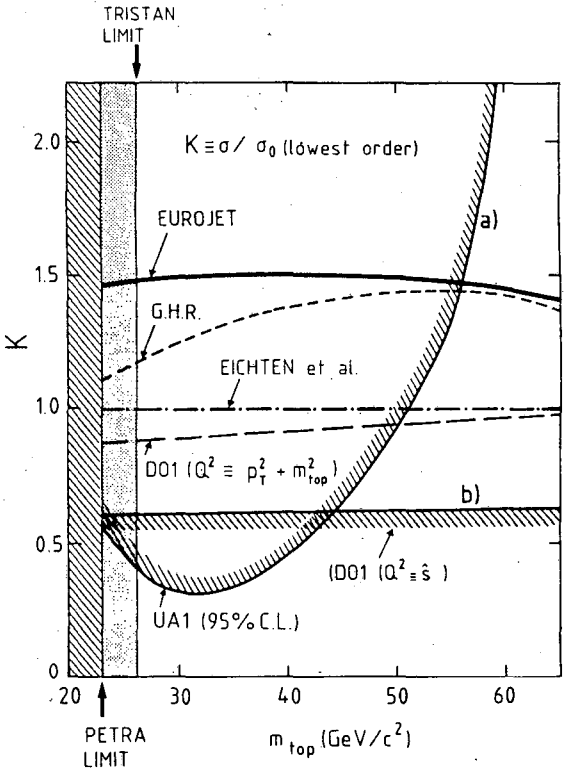

Fig. 20: The lower limit on M_t obtained by UA1. Curve (a) is the ratio of the experimental upper limit on $t\bar{t}$ production to the lowest order QCD production cross section with EHLQ1 structure functions and $Q^2 = M_t^2 + P_\perp^2$. Curve (b) is the ratio of theoretical expectations for $t\bar{t}$ production (lowest order) with DO1 structure functions and $Q^2 = \hat{s}^2$ to EHLQ1 with $Q^2 = M_t^2 + P_\perp^2$.

7.2 The UA1 Experiment in the 1988/1989 collider runs

During the 1988/89 CERN $p\bar{p}$ collider periods, UA1 intends to pursue its top search using its muon detection capability. The old electromagnetic calorimeters (gondolas and bouchons) have been dismounted and the replacement by the new

Uranium + TMP[40] calorimeter should not take place before the second half of 1989. The old hadron calorimeter is still in place, however. At present we are not able to trigger on electrons, thus the top decay channel into electrons is not available any more. The muon trigger and identification capability of the apparatus is however not substantially affected. In fact, the geometrical acceptance of the muon trigger is even increased by 30% with respect to previous data taking periods, and major improvements have been implemented on our trigger and data acquisition systems. The hadron calorimeter alone still provides adequate missing energy resolution, jet recognition and energy resolution for the medium $E_\perp$ jets encountered in the top search. A competitive top search in the muon decay channel is still possible.

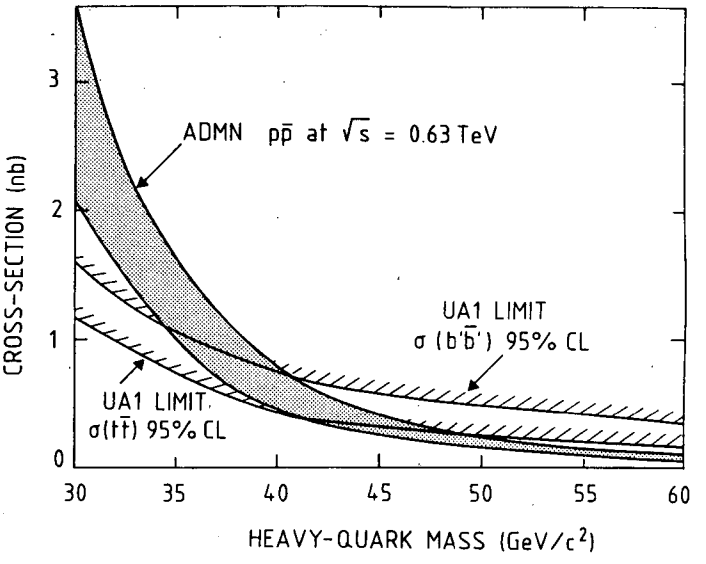

Fig.21: The band of theoretical expectations for $t\bar{t}$ production at 0.63 TeV from Ref. 7, compared to the experimental upper limit from UA1.

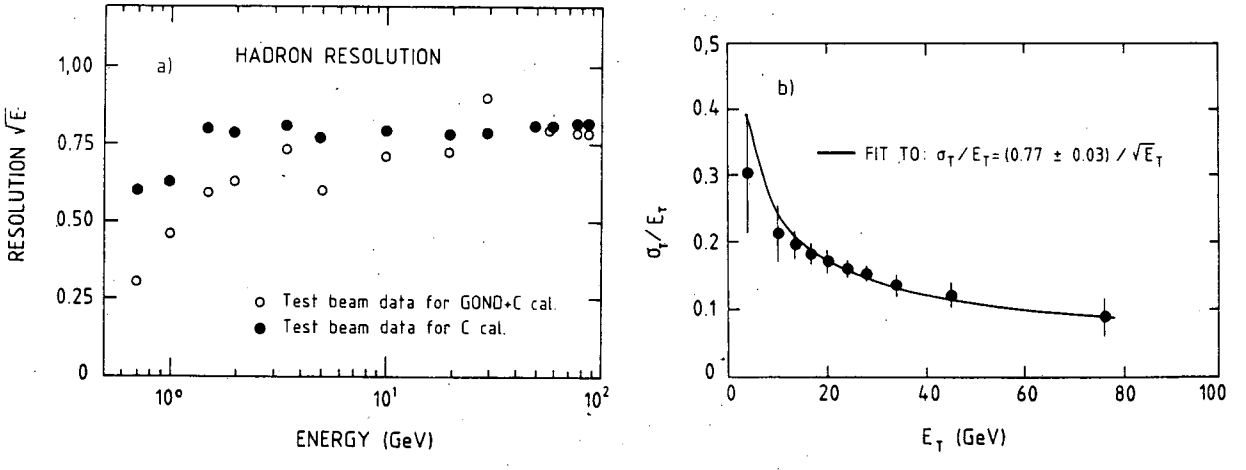

Fig. 22: a) Energy resolution of the present (old) hadron calorimeter alone (black dots) compared to that of the old electromagnetic + hadron calorimeter assembly (open dots). b)Missing transverse energy resolution with the stripped apparatus. The present resolution is $\sigma(\not{E}_T) = 0.77\ \sqrt{E_T}$.

Fig.22a shows the energy resolution ($\sigma(E)/\sqrt{E}$) of the present (old) hadron calorimeter alone (black dots), as measured in a test beam, in comparison to the hadronic resolution of the old electromagnetic + hadron calorimeter assembly (open dots). The degradation of the resolution is obvious, but the resulting resolution is adequate for jets of $E_\perp > 12$ to 15 GeV. The hadronic calorimeter is still largely 'hermetic', thus the degradation in the missing energy resolution is not very significant. This is visible from Fig.22b showing the missing $E_\perp$ resolution $\sigma(\not{E}_\perp)/E_\perp$ vs. $E_\perp$ where $E_\perp$ is the total scalar transverse energy in an event. This measurement is obtained from a large minimum bias data sample taken in 1987 with the stripped apparatus. The present resolution is $\sigma(\not{E}_\perp) = 0.77\sqrt{E_\perp}$, as compared to $\sigma(\not{E}_\perp) = 0.7\sqrt{E_\perp}$ with the old apparatus. As far as jet recognition is concerned, the improved azimuthal segmentation of the bare hadron calorimeter compensates in part for the loss in resolution.

UA1 thus feels confident that, with the muon trigger coverage of $|\eta| < 1.7$, no excessive π/K decay background for $P_\perp^\mu > 10$ GeV/c (the increase over the previous situation due to the longer potential decay path is < 30%) and with a jet recognition capability at $E_\perp^{jet} > 10$ GeV, the domain of top masses investigated could be further extended, up to $m_t \sim 60$ GeV with the luminosity foreseen for 1988/89. Fig. 23 shows some typical top decay ($t \rightarrow e/\mu\ b\ \nu$) kinematical distributions for $m_t = 50$ GeV. Notice that at $\sqrt{s} = 0.63$ TeV the dominant top production mechanism for $m_t >$ 45 GeV becomes $W \rightarrow t\bar{b}$, up to $m_t = 80$ GeV. Fig.23b shows the expected $P_\perp^\mu$ spectrum, the useful domain should be $P_\perp^\mu > 10$ to 12 GeV/c. Fig.23a shows the muon rapidity distribution for $p_\perp^\mu > 10$ GeV/c, which is to be compared to our single muon trigger acceptance of $|\eta| < 1.7$. Fig.23c shows the expected top decay b-quark transverse momentum.

The ACOL collider complex may be expected to deliver up to $4 pb^{-1}$ of integrated luminosity in 1988, and up to $10\ pb^{-1}$ by mid-1989. Fig.24 compares the UA1 sensitivity limits to the top quark at 0.7 events/pb from the present analysis using the muon decay channel only (shaded bands), with what may reasonably be expected for an actual (i.e. on tape) sensitivity of $4\ pb^{-1}$ in the present conditions with muon detection only. Fig.24 also shows the expected total + $t\bar{b}$ top production rate. With conditions and cuts similar to our present analysis, which was optimized for a 'light top' search, a sensitivity of $4\ pb^{-1}$ would allow us to investigate a domain of top masses extending up to ≈ 60 GeV. Notice that in this 45 to 65 GeV top mass

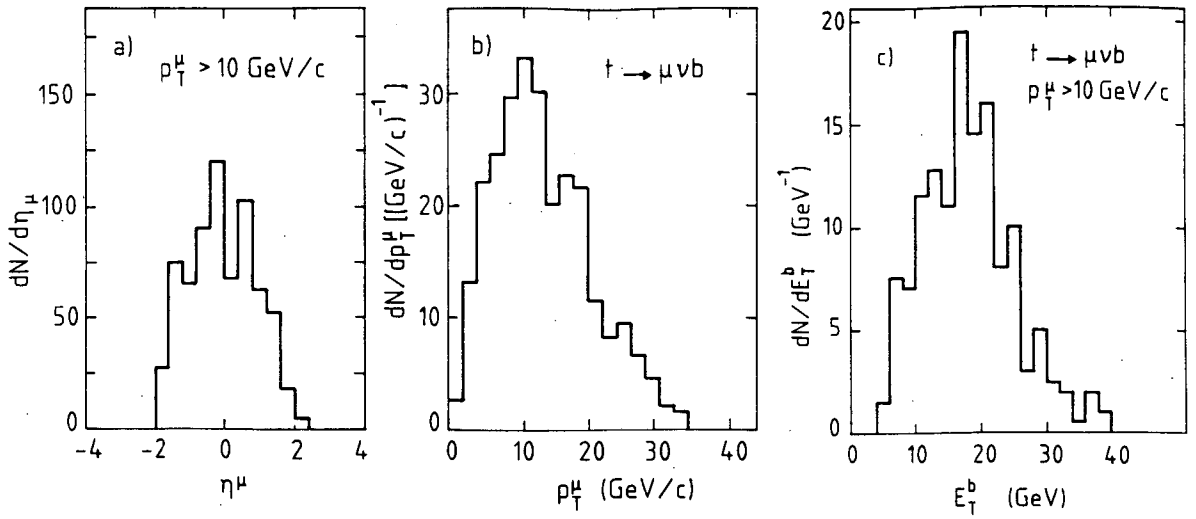

Fig. 23: Some top decay distributions for $M_t = 50$ GeV at $\sqrt{s} = 0.63$ TeV.

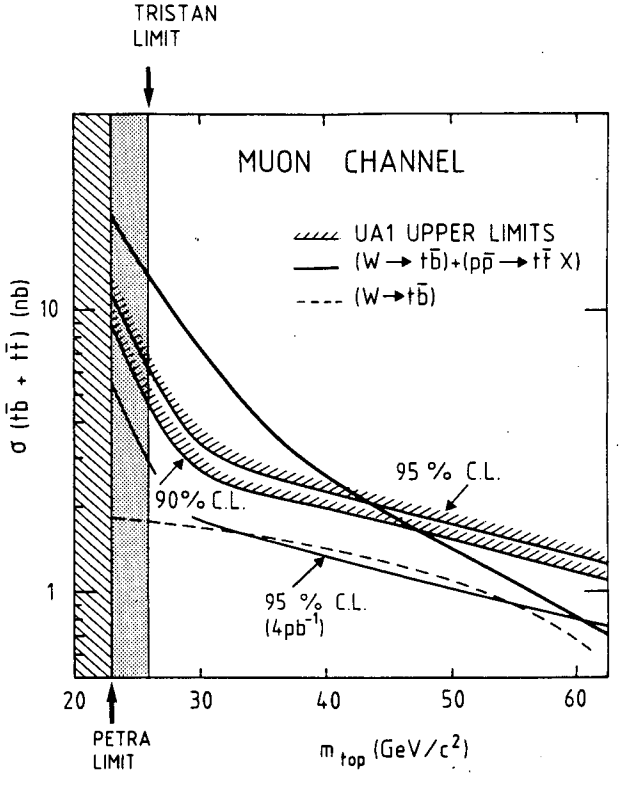

Fig. 24: Sensitivity limits to M_t of the UA1 experiment at integrated luminosities of 0.7 and 4 events/pb, from the top decay channel to muons only.

domain $W \rightarrow t\bar{b}$ production dominates, which has the double advantage of a simpler topology than for $t\bar{t}$ and a much more precisely known production rate, as it can now be normalized to the known $W \rightarrow e\nu$ cross section.

7.3 Top production and decay for $m_t \sim m_W$

It may be noticed from Fig.19 that for $m_t \sim m_W$ with a sensitivity of ~ 0.7 events/pb about 0.5 top events (per leptonic mode) might have already been expected,

and few promising events have indeed been seen[41,42]. The top search must be optimized for this mass region, in particular without excluding a priori $W \rightarrow \ell\nu$ consistent decays as done in a 'light top' search, and attempts must be made to detect the accompanying soft b-jets. In this mass range the top detection efficiency (excluding decay b-jets) is essentially that for large $P_\perp W$ production[43], i.e. $\varepsilon_W \approx 30$ to 40% . This top mass region is particularly interesting if a sensitivity of ≈ 10 events/pb can be achieved, in which case the CERN collider top mass reach extends up to ~ 100 GeV.

We now discuss a few characteristic features of top production and decay for $m_t \sim m_W$. The $p\bar{p} \rightarrow t\bar{t} \rightarrow W^+W^-b\bar{b}$ final state has a rather specific kinematics[41]. The experimental signatures are a large transverse momentum $P_\perp{}^t \sim P_\perp{}^W \sim m_t/2$, highly unbalanced transverse momenta of the two top decay products $P_\perp{}^W >> P_\perp{}^b$, and very dispersed and unbalanced W decay products, characteristic of large $P_\perp$ W production. Several spectacular events observed by UA1 and UA2[42,43] have indeed these properties and they might well be "early manifestations" of the top in this mass range[41a,42].

The top quark transverse momentum distribution $(1/\sigma)\, d\sigma/dP_\perp{}^t$ for several top masses at $\sqrt{s}$ = 0.63 and 2 TeV is shown in Fig.25. The average top transverse momentum is of the order of m_t. Due to the limited phase space available, the high $P_\perp{}^t$ tail at 0.63 TeV is significantly suppressed in comparison to $\sqrt{s}$ = 2TeV. In Fig.25 are also indicated the $P_\perp{}^t$ values for the special events of UA1/2, if these were interpreted as $t\bar{t}$ production.

The transverse momentum distribution $(1/\sigma)\, d\sigma/dP_\perp{}^b$ for the decay b quark is shown in Fig.26. It is in this variable that the crossing of the physical W decay threshold generates the most unusual behavior[41] . For $m_t < m_W$ the $P_\perp{}^b$ spectrum has an extended shape with a long tail. As $m_t \rightarrow m_W$ the distribution shrinks to reach a minimum $< P_\perp{}^b > \sim 10$ GeV at threshold, $m_t = m_W + m_b$. With m_t increasing further, the $P_\perp{}^b$ distribution starts to expand again. This is a well known kinematics (Lorentz boost) effect (present for example in energetic $\Lambda \rightarrow p\pi$ or $\Xi \rightarrow \Lambda\pi$ decays of the old days!) in decays with small decay Q-values. The momentum is shared between the $t \rightarrow Wb$ decay products in the ratio $P_\perp{}^b/P_\perp{}^W \rightarrow m_b/m_W$ as $Q \rightarrow 0$. Most of the large top transverse momentum $P_\perp{}^t$ is thus taken over by the decay W and the b jets are difficult to observe being very soft. Fig.27a shows the scatter plot of $P_\perp{}^b$ vs. $P_\perp{}^W$ for m_t = 90 GeV at $\sqrt{s}$ = 0.63 TeV, and Fig.27b for m_t = 150 GeV at $\sqrt{s}$ = 5 TeV. The unequal sharing of transverse momenta between the decay W and b for $m_t \sim m_W$ is particularly striking in these plots. The effect is however localized to $m_t \sim m_W$, as for

m_t = 150 GeV (Fig.27b) there is almost equipartition of transverse momenta. This is important for the Fermilab collider regime where for a sensitivity of 10 events/pb the top mass reach extends up to ~ 150 GeV. The appearance of the decay b-jets may allow additional background (single W + jets) rejection criteria to be applied.

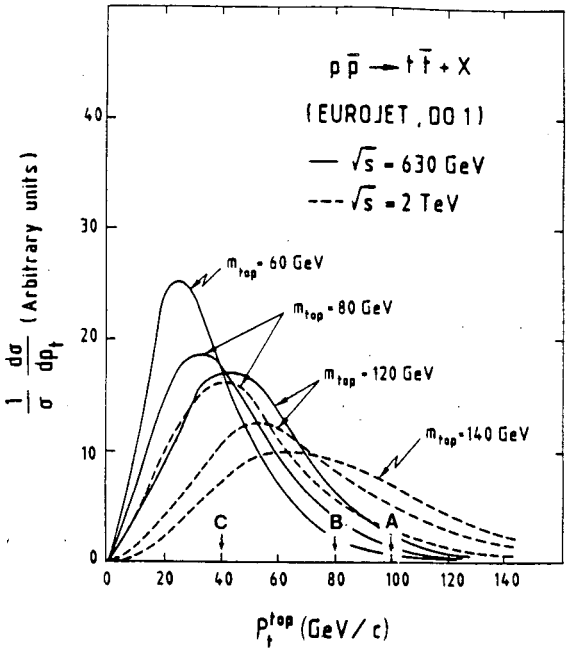

Fig. 25: Normalized top transverse momentum distribution at $\sqrt{s}$= 0.63 and 2 TeV, for $m_t \sim m_W$.

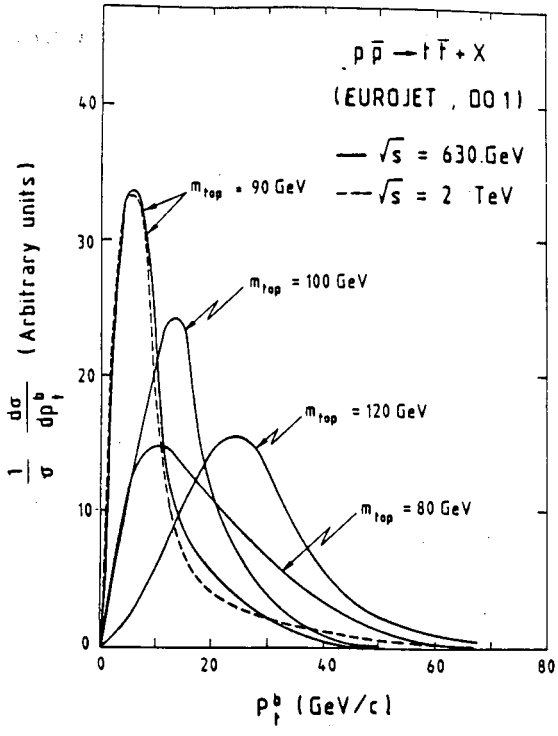

Fig. 26: Normalized b-quark transverse momentum distribution at $\sqrt{s}$ = 0.63 and 2 TeV.

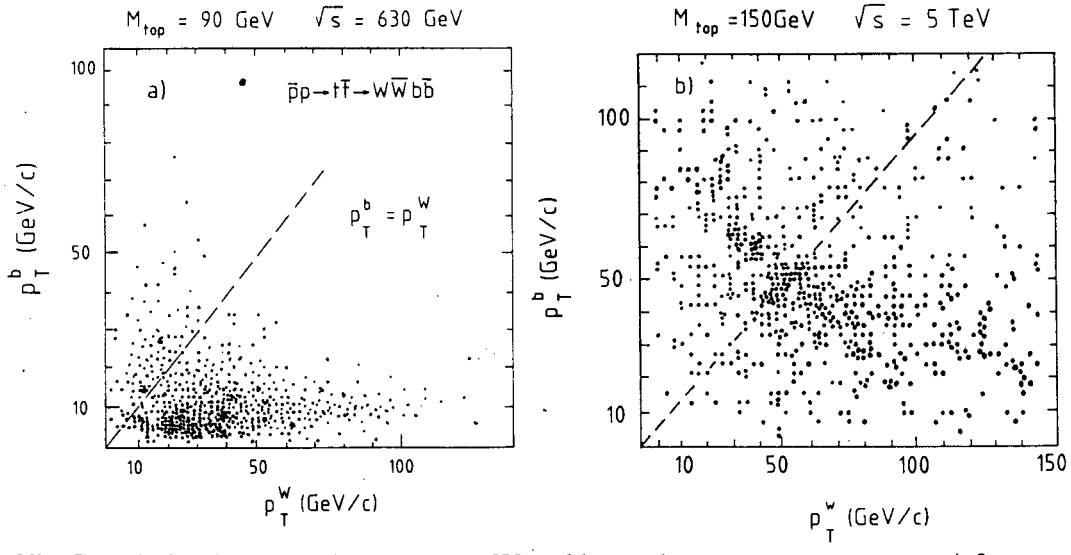

Fig. 27: Correlation between the top decay W and b-quark transverse momenta, a) for m_t = 90 GeV at $\sqrt{s}$ = 0.63 TeV, and b) for m_t = 150 GeV at 5 TeV.

Another interesting feature concerns the W decay products ℓ-ν or q-$\bar{q}$. While at low $P_\perp^W$ the $W \rightarrow \ell\nu$ decay products exhibit a strong correlation $E_\perp^\ell \sim E_\perp^\nu$ with a pronounced "Jacobian peak"[43], for W's produced with large $P_\perp$ this correlation disappears. As visible from Fig.28 it is replaced by an opposite correlation. This is due to a large mass, large $P_\perp$ object decaying into two ~ massless particles, with their transverse momenta being measured with respect to the $p\bar{p}$ beam line, and not the parent W line of flight. In Fig.28 are also indicated the kinematical configurations of the apparent WW events of UA1/2, and the typical detection thresholds of $E_\perp^{\ell,\nu} > 15$ GeV. It is obvious that raising the lepton and/or neutrino threshold to 25 GeV introduces a large loss of efficiency for such events.

Fig.29 shows the total $t\bar{t}$ + $t\bar{b}$ production cross section at $\sqrt{s}$ = 0.63 and 1.8 TeV, and their ratio, as a function of m_t. The message is clear: for $m_t > 80$ GeV the Fermilab collider has a substantial advantage in $t\bar{t}$ production rate (a factor > 20) over the CERN collider. For smaller top masses $50 < m_t < 75$ GeV top production is in fact dominated by $W \rightarrow t\bar{b}$ production and the relative advantage of Fermilab is less pronounced, a factor 4 to 10.

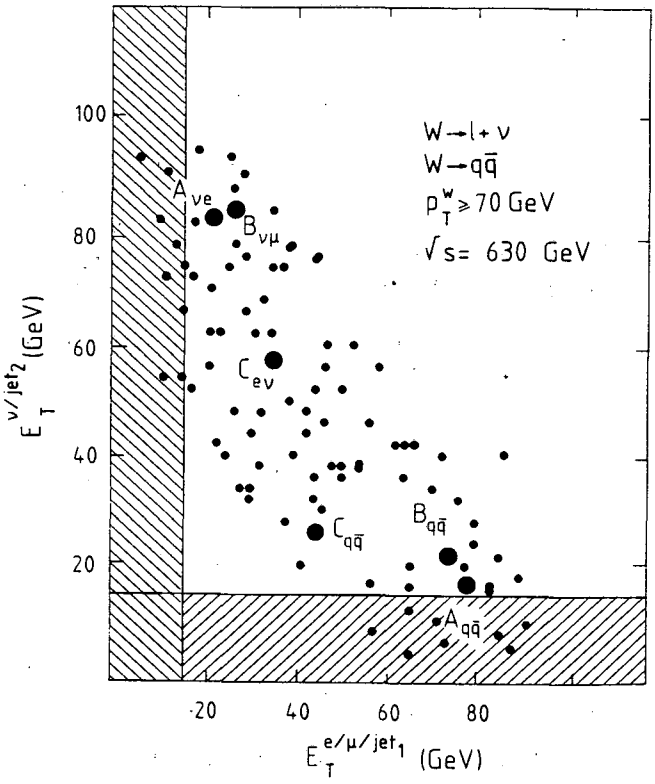

Fig. 28: Correlation between the transverse energies of the two leptons (or the two quarks) from a W decay, for W's produced at large $P_\perp$.

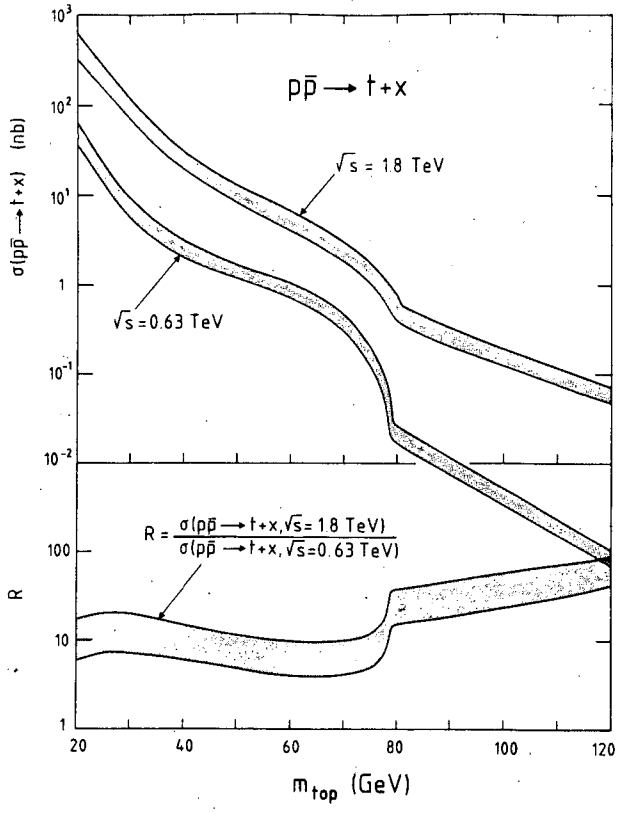

Fig. 29: The $p\bar{p} \rightarrow$ top production cross section (from both $t\bar{t}$ and $t\bar{b}$ mechanisms) as a function of m_t at $\sqrt{s}$ = 0.63 TeV and 1.8 TeV.

7.4 The special events of UA1/2

From the left-hand scale of Fig.19, with a W ($\rightarrow \ell\nu$) detection efficiency[43] of $\varepsilon_W \approx 0.3$ at large $P_\perp{}^W$, from ~ 0.7 to ~ 0.2 events per W leptonic mode can be expected for m_t in the ~ 75 to ~ 90 GeV range, without any "stretching" of QCD expectations[41]. In this context it is interesting to recall that UA1 has observed two[42] and UA2 one[44] $W \rightarrow \ell\nu$ event accompanied by two hard jets with $m_{jet\text{-}jet} \sim m_W$. These events are suggestive of $t\bar{t}$ production in the $m_t \sim m_W$.

The event of UA2 (labelled C in Fig. 28) is the only W + 2 jet event within the acceptance of UA2 ($|\eta_{jet}| < 0.85$ and $E_\perp{}^{jet} > 10$ GeV). In this event $P_\perp{}^W \sim 40$ GeV/c and with $P_\perp{}^W \sim P_\perp{}^t$ in the $t\bar{t}$ interpretation, it falls at about the most probable $P_\perp{}^t$ according to Fig.25. The jet-jet effective mass is ~ 60 GeV, somewhat low in comparison to m_W, but cannot be excluded on a particular event. According to UA2, the production rate and the accompanying 2-jet kinematical configuration of this event is also entirely consistent with second order QCD corrections to single W production[45].

UA1, in a larger jet acceptance ($|\eta_{jet}| < 3.0$ and $E_\perp^{jet} > 7$ GeV), has 10 W + 2 jet events, for a total $W \rightarrow e\nu$ sample of ~ 300 events. The only two WW consistent UA1 events (labelled A and B in Fig. 28), have been widely discussed[42]. They are the two largest $P_\perp^W$ events in the UA1 sample, with $P_\perp^W \geq 65$ GeV. The internal lepton-lepton and jet-jet decay configuration, with its characteristic $E_\perp$ unbalance, is entirely consistent with expectations for large $P_\perp^W$ production (Fig.28). The problem for the $t\bar{t}$ interpretation is the unusually high value of the observed $P_\perp^W$. These two events represent a rather unlikely sampling of the expected $P_\perp^W$ (or $P_\perp^t$) distributions for $t\bar{t}$ production (Fig.25). At the observed $P_\perp^W$ values the $t\bar{t}$ production rate is ≤ 0.07 events. However, the resolution on $P_\perp^W$ is ~ 15% for large $P_\perp^W$, the systematic uncertainty on the absolute energy scale is ~ 9% and the event probability is a very sensitive function of $P_\perp^W$.

The single W + 2 jets background has also been extensively studied by UA1[42]. The problem for these two events is again too large values of $P_\perp^W$. The situation is best summarized by Fig.30a showing the scatter plot of the effective mass M(W-jet$_1$-jet$_2$) vs. $P_\perp^W$ for all UA1 W + 2 jet events[42]. The event population is compared to the expected QCD W + 2 jet production. It is properly clustered in the expected most probable region of the plot with the two events A, B rather separated from this population. They may be a tail sampling from this QCD population, but the expected number of events[42] in this kinematical configuration is ~ 0.05. The corresponding M(W-jet-jet) vs. $P_\perp^W$ plot for events A, B and C for the hypothesis is shown in Fig.30b. The contours correspond to UA1 acceptancies and detector simulation[46], but event C can be meaningfully incorporated in such a comparison. The sampling of the expected $t\bar{t}$ population in Fig.30b provided by the three events together, however, is not so bad.

In conclusion, the probability of the $t\bar{t}$ interpretation of these few events is as good as any other found until now. Only higher statistics with a good understanding of rates and event configurations of the W + ≥ 2 jet background could definitely confirm or reject the $t\bar{t}$ production hypothesis. A detailed experimental and theoretical understanding of W production at large $P_\perp$, with associated jet multiplicities and event configurations, will be needed before top production in this mass range could be ascertained at $\sqrt{s}$ ~ 2 TeV, despite the big advantage in production rate. The forthcoming CERN and Fermilab collider periods, where ~ 10 events/pb can be expected by the end of 1989, could clarify the situation.

7.5 The possible upper limit on m_t from $(\sigma \rightarrow \ell\nu)/(Z \rightarrow \ell\ell)$

A significant result concerning m_t might come first from the improved measurements of the ratio of $W \rightarrow \ell\nu$ to $Z^\circ \rightarrow \ell\ell$ cross sections at CERN or Fermilab collider experiments. This ratio:

$$R = \sigma(W \rightarrow \ell\nu)/\sigma(Z \rightarrow \ell\ell) = \sigma_W/\sigma_Z \, BR(W \rightarrow \ell\nu)/BR(Z \rightarrow \ell\ell),$$

is sensitive[47,48] through the W, Z leptonic branching ratios to additional open channels, like $W \rightarrow t\bar{b}$ or $Z \rightarrow t\bar{t}$. R depends significantly on the top quark mass, if $45 < m_t < 75$ GeV, as for $m_t < 45$ GeV both the $Z \rightarrow t\bar{t}$ and $W \rightarrow t\bar{b}$ channels are open, while for $45 < m_t < 75$ GeV only $W \rightarrow t\bar{b}$ remains. An upper limit on the top quark mass might be obtained from the comparison of the directly measured value of R to its theoretical expectation. The latter one can be expressed in terms of the total and partial widths of the W and Z° as follows:

$$R_{th} = \left[\frac{\sigma_W}{\sigma_Z}\right] \cdot \left[\frac{\Gamma_{e\nu}{}^W \, \Gamma_{tot}{}^Z}{\Gamma_{ee}{}^Z \Gamma_{tot}{}^W}\right] = R_\sigma . R_\Gamma \, (m_t, \Delta N_\nu)$$

The ratio of total production cross sections R_σ can be reliably calculated in QCD and is a slowly varying function of $\sqrt{s}$, while the second term R_Γ is predicted by the electroweak Standard Model. It contains all the dependence[48] on the top quark mass and the number of neutrino families through the ratio $\Gamma_{tot}{}^Z \Gamma_{tot}{}^W$.

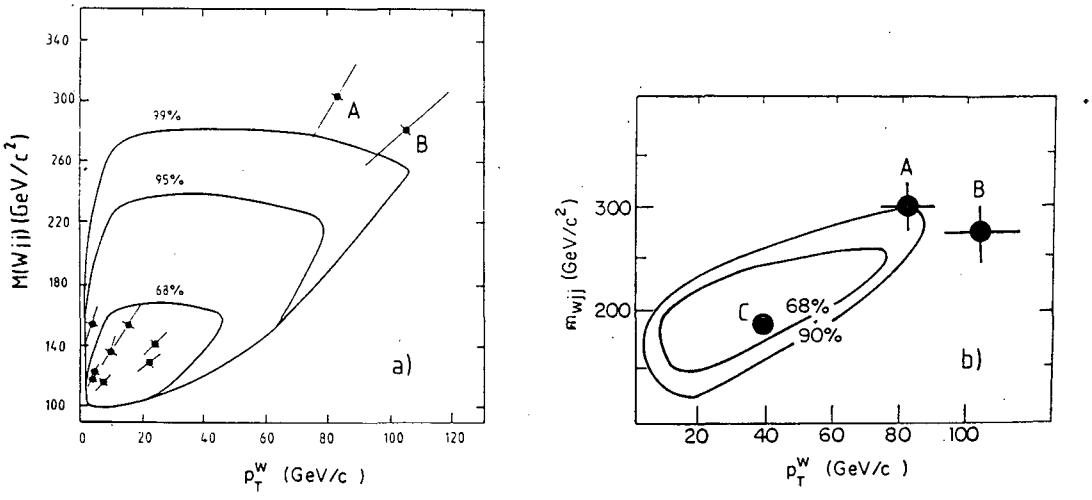

Fig. 30: a) Scatter plot of the W-jet-jet effective mass vs. $P_\perp{}^W$ for the UA1 W + 2 jet events with the expected QCD distribution. b) Scatter plot of the W-W effective mass vs. $P_\perp{}^W$ for $t\bar{t}$ production[46].

The expected variation of $R = R_\sigma R_\Gamma$ as a function of m_t for $N_\nu = 3$ and 5 is shown in Fig.31 for a value $R_\sigma = 3.25$, with the hatched band showing the effect of the theoretical uncertainty[48] $\delta R_\sigma = \pm 0.1$. A lower value of R_σ is clearly less constraining for m_t. The prediction is compared to the present combined UA1/2 experimental central value of R and the upper limits at 90% and 95% C.L. Fig.31 shows clearly that for large top masses the constraint is strong, but not yet such that $m_t > m_W$ can be excluded at a 95% C.L.[48,49]

The uncertainties on the present measurements of R are predominantly of statistical origin, due to the limited number of Z° events[49]. A significant improvement on this measurement can thus be expected in the near future, and the CERN and Fermilab collider experiments, with ~ 10 events/pb by the end of 1989, by this method could definitively settle the question whether or not $m_t < m_W$.

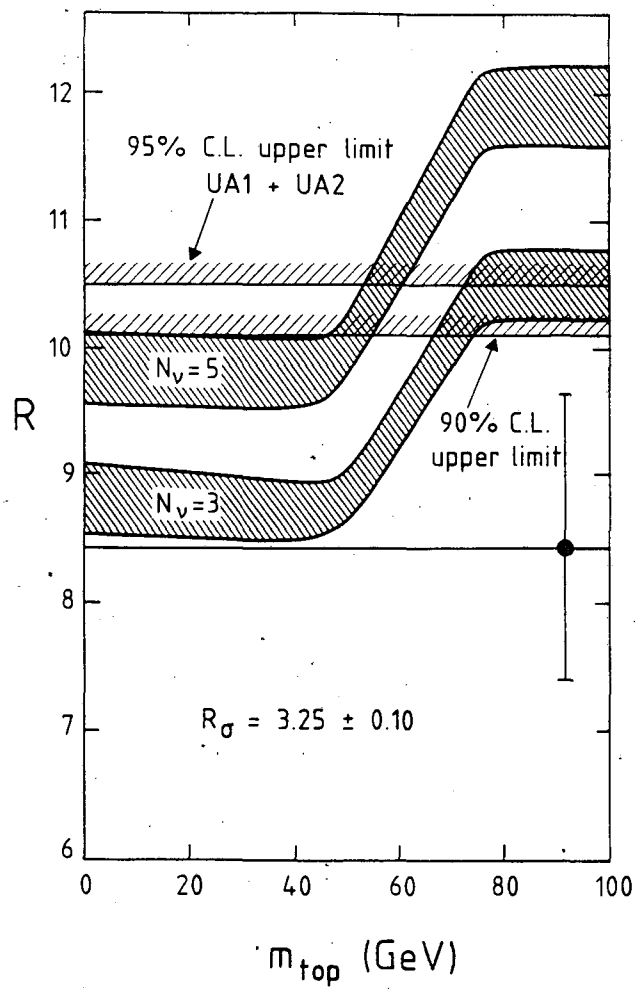

Fig. 31: Comparison of the expected variation of $R = \sigma(W \rightarrow \ell\nu)/\sigma(Z \rightarrow \ell\ell)$ as a function of m_t for $N_\nu = 3$ and 5 with the value of R measured by UA1/2. The shaded band shows the theoretical uncertainty on this ratio. N_ν is the number of light neutrino species.

8. Top Search at CDF

The CDF detector has collected an integrated luminosity of 25 nb^{-1} in the 1987 Tevatron Collider run[50], which was not sufficient for top searches. We are presently taking data with a luminosity of 10^{30} cm^{-2} sec^{-1} and expect 2 - 5 pb^{-1} to be collected in the 1988-89 run (the initial plan was for 1pb^{-1} in this running period).

The main production mechanism at 1.8 TeV is the one of Eq.6.2, i.e. $p\bar{p} \rightarrow t\bar{t}$ + X, via gluon fusion and $q\bar{q}$ annihilation. The rate for $W \rightarrow t\bar{b}$ is smaller than that for pair production at all top masses, except for $m_t \sim 60$ GeV (see Fig. 4). The cross sections are clearly larger at 1.8 TeV than at 0.63 TeV, by large factors, 5 - 30, as it is illustrated in Fig. 29. For a top mass above 70 GeV, CDF has a clear advantage over the CERN experiments, for the planned data runs.

As discussed in Sec. 2, the cross section uncertainties on top production are of the order of 30%. Using the cross sections from Altarelli et al[7], we, expect at different energies, the number of $t\bar{t}$ pairs produced shown in Table 5 .

Table 5: Cross sections[7] and number of $t\bar{t}$ pairs expected at $\sqrt{s}$ = 1.8 TeV.

m_t (GeV)	$\sigma(p\bar{p} \rightarrow t\bar{t}X)$ (nb)	$t\bar{t}$ pairs produced for $\int Ldt = 1pb^{-1}$
40	$9.63^{+1.7}_{-2.5}$	7100 - 11300
60	$1.27^{+0.19}_{-0.35}$	920 - 1460
80	$0.285^{+0.037}_{-0.077}$	210 - 320
100	$0.087^{+0.011}_{-0.023}$	60 - 100
120	$0.033^{+0.003}_{-0.009}$	25 - 37

These rates of production will allow CDF to use dilepton topologies for the lower masses. This is a clear advantage as background rates are lower for the channels e^+e^-, $e^+\mu^-$, or $\mu^+\mu^-$. The major background would be from $b\bar{b}$ production in all cases,

whereas for same flavor dileptons the Drell-Yan dilepton production background has to be taken into account.

For higher masses, the topology "isolated lepton + jets" would be the one of choice. In this case we have

$$\bar{p}p \rightarrow t\bar{t} + X \qquad (8.1)$$
$$\quad\; \lfloor\!\rightarrow (\ell\nu)\,\bar{b}$$
$$\quad\; \lfloor\!\rightarrow (u\,\bar{d})\,b$$

a lepton and at least four jets would be expected. However, the $P_\perp$ distributions of these jets depends on the top mass and quite often only two would be observed. In fact, quark fragmentation at low energies would spread the jet over a large area, so that, in the presence of underlying event and gluon radiation, it would be difficult to detect.

The $P_\perp$ distribution[51] of the bottom jets is shown in Fig. 32 for different top masses. Clearly the kinematics changes as the top mass reaches the W mass, as already discussed in Sec. 7.3. At this energy the 3-body decay of Equation 8.1 becomes a two body decay, because the W is real. The b quark, being much lighter than the W, will have very little $P_\perp$. A more detailed study of this topology will be discussed in Sec. 8.3

In CDF the muon coverage is only partial ($|\eta| < .65$ in the central region), whereas the electron coverage extends to all the rapidity region for necessary top production ($|\eta| < 3$). Therefore, we will concentrate here on the electron analysis. Fig. 33 shows the inclusive $P_\perp$ spectrum for electrons produced in the $b\bar{b}$, $t\bar{t}$ and W final states[51]. Several top masses are shown. These spectra include only the branching ratio into electron, 100% detection efficiency is assumed. The EHLQ1 structure functions are used and the choice of scale is $Q^2 = P_\perp^2 + m^2$.

It is clear that electrons from b productions are many orders of magnitudes than those from top. The b production mechanism used for the calculation of Fig. 33 is a $2 \rightarrow 3$ process[52] which includes: $gg \rightarrow b\bar{b}g$, $gq \rightarrow b\bar{b}q$, and $qq \rightarrow b\bar{b}g$. The total cross section for b pair production at 1.8 TeV is in the range of 30 - 60 μb (see Fig. 5). For low mass top this is the major source of background from real electrons.

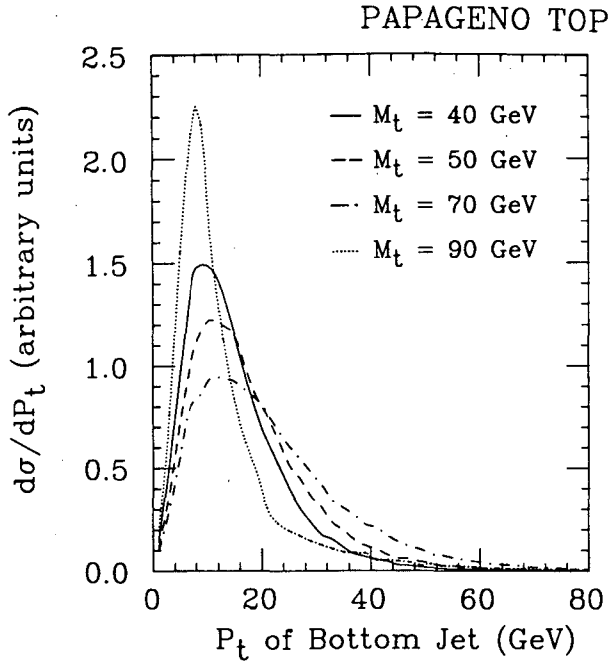

Fig. 32: $P_\perp$ spectrum of the bottom jet from top decay at various top masses.

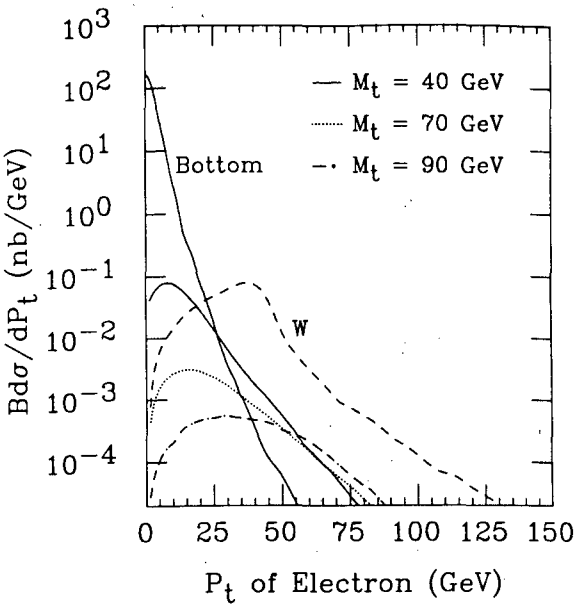

Fig. 33: Inclusive $P_\perp$ distribution of the electron from top and bottom semileptonic decays and for $W \rightarrow e\nu$. Only the branching ratio into electron has been included in the rate.

Another source of background is due to electron misidentification, i.e., pions or photons from QCD processes that fake electrons. This,we discuss next.

8.1 Electron Identification in CDF

Description of the CDF detector can be found in Ref. 53. We outline here the selection criteria for electrons in the central calorimeter, similar criteria can be applied for the rest of the solid angle.The central calorimeter ($|\eta| < 1$) electron identification is based on information from the calorimeter towers (segmentation is $\Delta\eta = 0.1$ and $\Delta\phi = 15^o$), and information from strip chambers. These are located at the maximum of the electromagnetic shower, and measure the shower position and pulse height in two dimensions. Requirements are based on:

a. ratio of hadronic to electromagnetic energy,
b. consistency of shower shape in calorimeter towers to test beam data,
c. matching of shower position in the strip chambers with that expected, from the track measured in the central tracking chamber (CTC),
d. consistency of strip chamber pulse heights with test beam data,
e. matching of energy in calorimeter with the measured momentum in the central tracking chamber.

f. isolation, which uses the $\Delta\eta$, $\Delta\phi$ segmentation of the calorimeter.

This type of analysis except for requirement d., has been performed to study W production[54]. Plots of some of the above variables are shown in Fig.34.

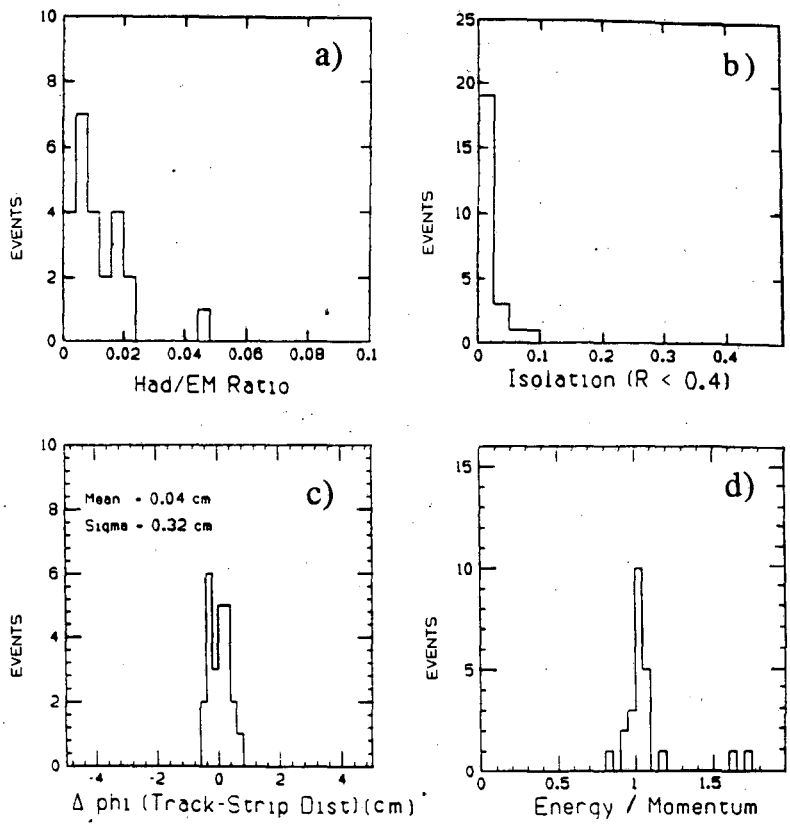

Fig. 34: Electron selection variables in the CDF (1987 data) W sample. a) the ratio of hadronic to electromagnetic energy, b) the isolation, c) the matching in ø between the calorimeter cluster and extrapolated track position, and d) the ratio of the energy of the cluster to the track momentum (E/p).

For the top studies we plan to put more stringent requirements than for the W sample. We will have plenty of statistics to optimize the cuts. These will have to remove backgrounds from $\pi^+\pi^o$ overlaps, conversion pairs (there will be additional requirements on the charged tracks measured in the CTC in the vicinity of the electromagnetic shower), and charged pions interacting early in the e.m. calorimeter. The present estimate is that the background will be less than 30%.

8.2 Bottom Quark Background

For low mass top, the electron rate from b pair production is dominant. The electrons from b decays, however, are generally not isolated, so the background shown in Fig.33 can be reduced substantially by applying an isolation cut.

A preliminary study has been done by generating the reaction $\bar{p}p \rightarrow b\bar{b}$ in ISAJET[55] and then using our detector simulation and analysis package. These events are only part of the processes that contribute to bottom production, the major

contribution, about a factor 3 larger, being bottom pairs from gluon splitting, the process which was used for the spectrum shown in Fig. 32. A study of this process with ISAJET and detector simulation is in progress. These electrons, however, are expected to be strongly suppressed by the isolation cut, since the two b's will not be back to back.

The present study shows that, starting with a $b\bar{b}$ cross section of 23 μb, the electron cuts and the requirement of 2 clusters in the event with $E_T > 7$ GeV, eliminate most of the events except for a small number, equivalent to an observed cross section $\sigma_{obs} = 0.48$nb.

Fig. 35 shows the electron $P_\perp$ spectrum for these events. Also shown is a sample of $\bar{p}p \rightarrow t\bar{t}$ events for $m_t = 40$ GeV, that went through the same analysis. For the top sample $\sigma_{obs} = 0.45$ nb, however, the spectra are quite different and a cut at 10 GeV leaves little background under the top signal.

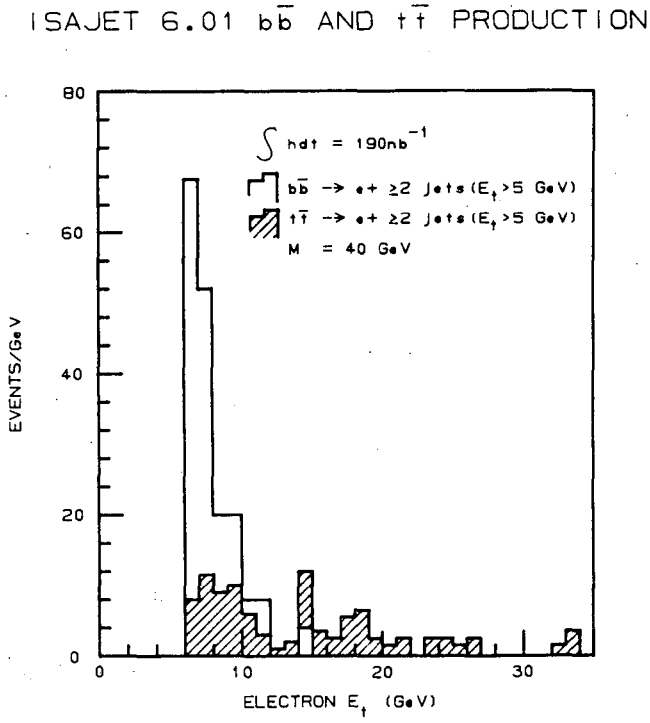

Fig. 35: The electron E_T spectrum for observable $b\bar{b}$ (unshaded) and $t\bar{t}$ (shaded) events. Obtained using ISAJET, the CDF detector simulator and the analysis described in the text.

Clearly more detailed studies need to be done, and all b production processes need to be simulated. We expect that the background from the $2 \rightarrow 3$ processes can be considerably reduced by the isolation requirement on electron candidates. Of course, as discussed in Sec. 2, the b cross section is quite uncertain. We will have to measure it at 1.8 TeV and understand the characteristics of the b events in the CDF detector.

8.3 W + Jets

Fig. 36 shows the $P_\perp$ spectrum for electrons from W production. Most of the W's have low $P_\perp$ and are not associated with jets. Since top events tend to have high jet multiplicities, we have studied in more detail the processes

$$p\bar{p} \rightarrow W + 1 \text{ jet}$$
$$p\bar{p} \rightarrow W + 2 \text{ jets}$$

for which matrix elements have been calculated.[56,57] These matrix elements diverge at low $P_\perp$ and special care should be taken in using them. Exact calculations of the $P_\perp^W$ spectrum have been done by Altarelli et al.[58], taking into account all higher order processes and all necessary cancellations. With $P_\perp$ cuts on the produced jets, the matrix elements of Ref. 56 and 57 are expected to be adequate.

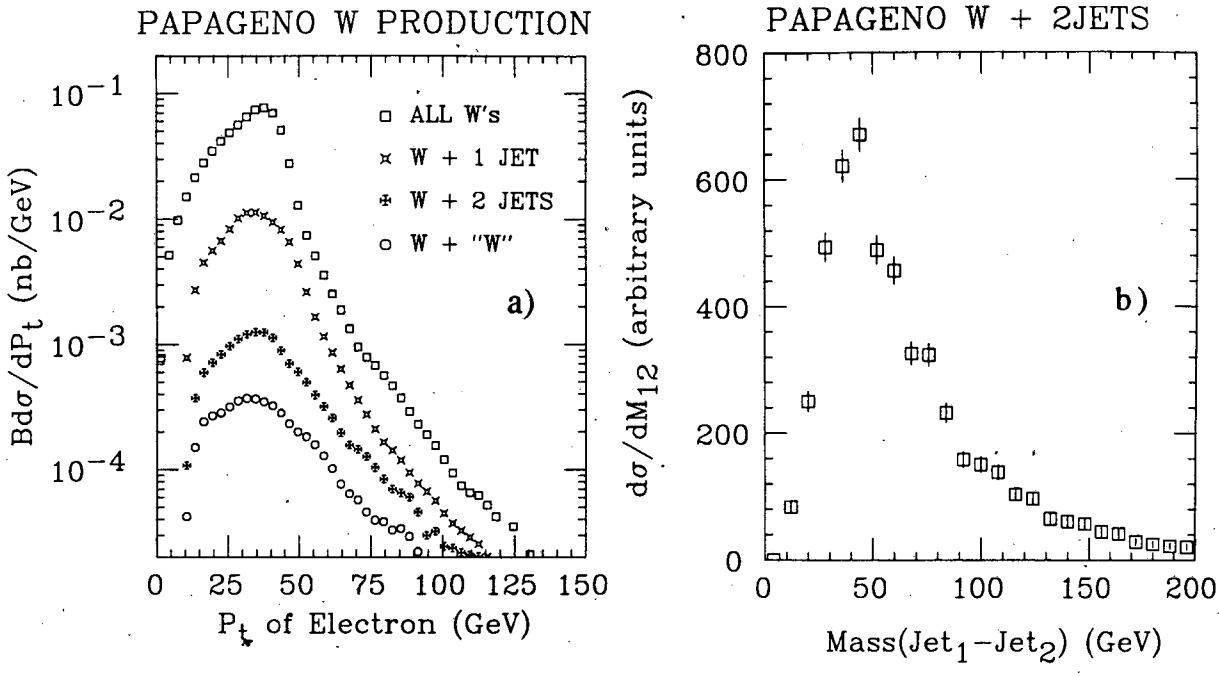

Fig.36: a) Inclusive $W \rightarrow e\nu$ production cross sections at 1.8 TeV. The curve labelled ALL W's, has no cuts. The jet requirements are explained in the text. The curve labelled W + "W" requires the two jet mass to be in the interval $M_{12} = 80 \pm 25$ GeV. b) Invariant mass of the two observed jets. This and subsequent figures are obtained using the program PAPAGENO.[51]

A preliminary study of the W + jets backgrounds have been made with parton level calculations using PAPAGENO[51] (which uses the matrix elements of Ref. 56 and 57), and crude estimates of detector efficiencies. Cuts on electron and jets are as follows:

a. electron cuts

$$P_\perp^e > 12\ \text{GeV} \qquad |\eta| < 2.0 \qquad (8.2)$$

b. jet cuts

$$E_\perp^{jet} > 15\ \text{GeV} \qquad |\eta| < 3.0 \qquad (8.3)$$

$$\Delta R > 0.8 \qquad \text{for Njets} \geq 2 \qquad (8.4)$$

where ΔR is the radius in $\Delta\phi$ and $\Delta\eta$ for two jets to be found as separate clusters by the CDF cluster algorithm. The 15 GeV jets appear in CDF as cluster with an average energy around 10 GeV in a cone of $\Delta R = 0.7$. The η cuts are imposed to reduce QCD background.

Fig. 36a shows the distribution of the $P_\perp$ of the electrons from W's. Only the $W \rightarrow e\nu$ branching ratio is included in the total rate, whereas the above cuts have been used for the other curves. The production rate is reduced by a large factor when two observed jets are required. The invariant mass of the jets is shown in Fig. 36b. For $m_t \sim m_W$, we expect two W's in the event, so it is interesting to see how often the two jets are close to the W mass. The curve W + "W" shows the electron spectrum for the events with M (jet 1 + jet 2) = 80 ± 25 GeV, where a preliminary estimate, σ = 13 GeV, of the two jet mass resolution at the W has been used.

The total rates are shown in Table 6. We reiterate that only the requirements of Eq. 8.2 - 8.4 are included in the calculations, no detector acceptances are taken into account. Note that, taking into account detector resolution the W + "W" cross section is larger than the $\bar{p}p \rightarrow WW$ production ($\sigma = 2 \pm 1$pb) by a large factor.

Next we do the same analysis on top events at different masses. The same requirements (EQ. 8.2 - 8.4) are imposed on the electrons and the jets. The observed s.B for five different top masses, and for different number of jets are shown in Table 6.

We now compare the electron spectrum for W + jets and top production for different topologies. Fig. 37 shows the electron + 1 jet spectra. Clearly the W production is much larger than the top at all except the 40 GeV top mass. Fig. 38 shows the same spectra for the 2 jet case. Again the W + 2 jets dominates the 2 jet topology, except for 40 GeV top where the electron spectrum is softer than for W.

Table 6: Inclusive electron cross sections for W and top production Requirements are: electron $P_\perp >$ 12 GeV, jet $P_\perp > 15$ GeV, jet separation (in η,ϕ) $\Delta R = 0.8$ for two or more jets. The η cuts are shown in Eq. 8.2 - 8.4. All rates are calculated using the Montecarlo program PAPAGENO[51].

	Total[a] e + n jets σ.B(pb)	e + 1 jet σ.B (pb)	e + 2 jets σ.B (pb)	e + > 2 jets σ.B (pb)
40	1310	246	68	130
60	188	24	20	74
70	86	7.7	10	45
90	23	3.8	7.8	10.9
100	14.5	0.6	1.1	11.4
All W's	2000			
W + 1 jet[b]	423	330		
W + 2 jets[b]	79		44	
W + "W"			15	

a. No cuts are applied here: n ≥ 0jets, all electrons are included.
b. Jet $P_\perp > 10$ GeV required for total cross section calculation.

For $m_t = 60$ GeV, the W background is already larger than the top signal in the 1-jet or 2-jet topologies.

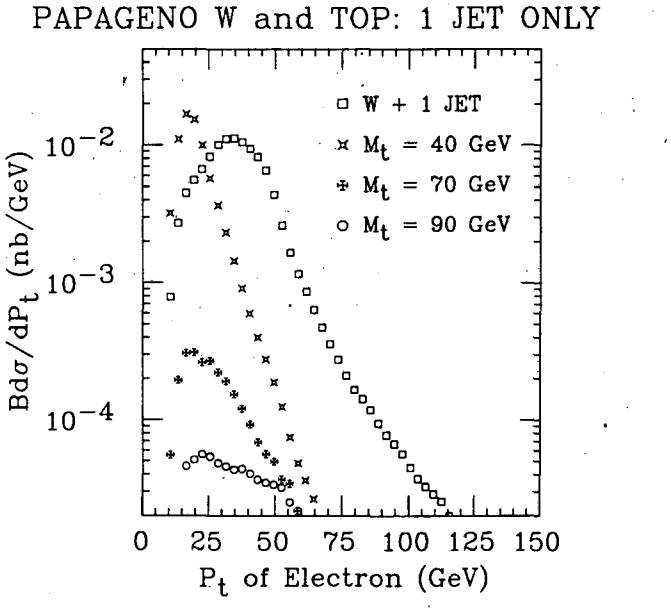

Fig. 37: Inclusive electron $P_\perp$ spectra for the electron and one jet topology. Curves refer to W and top production at several masses (see text).

The W + 3 jet production has not been calculated at this point, and we do not have any estimate of its cross section. But, assuming that it is not larger than the W + 2 jet cross section, from Table 6 we expect to be able to use the e + 3 jets topology to separate top from W, up to $m_t \sim 60$ GeV.

As we approach the W mass, the situation becomes more complicated. W production dominates top production. Fig. 38b shows that at $m_t = 90$ GeV the W + "W" rate is about twice that of the top signal. Clearly just the production rate and the $P_\perp$ spectrum are not enough to detect a top signal. At masses $m_t \sim m_W$ one possible handle is the detection of the b jets, which are very soft. Any other variable, a priori, seems to be the same for the two cases.

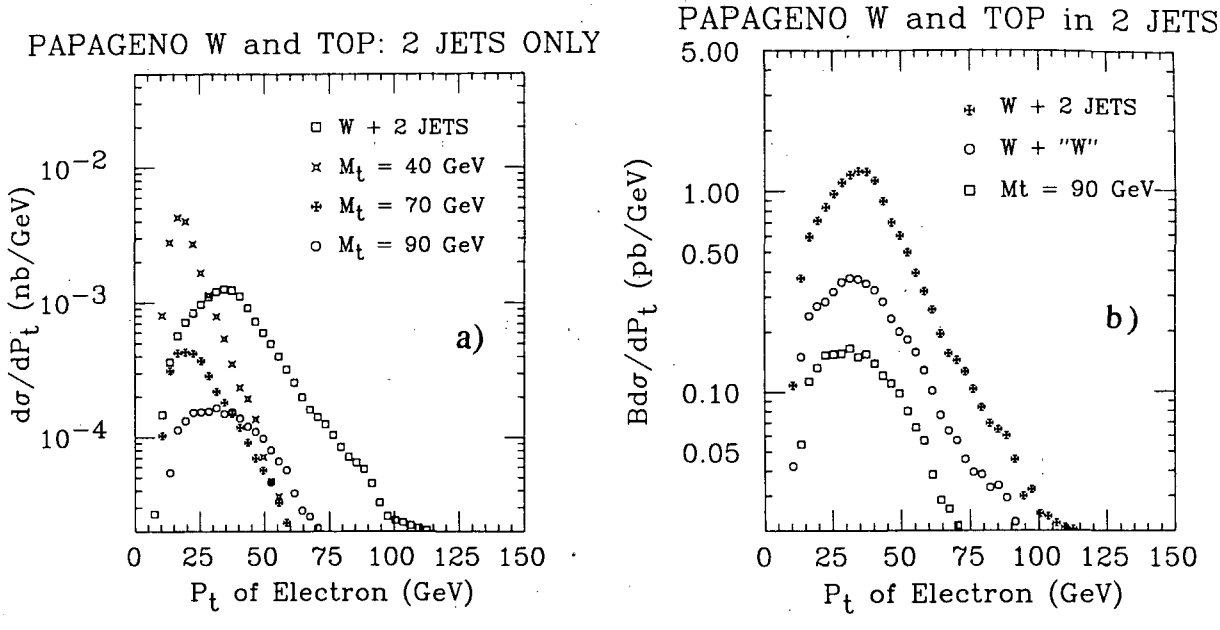

Fig. 38: Inclusive electron $P_\perp$ spectra for the electron and two jet topology a) W + 2 jet and three different top masses, b) W + 2 jets, W + "W", i.e., the tow jets are required to be in the interval $M_{12} = 80 \pm 25$ GeV and $m_t = 90$ GeV.

In summary, the background from W + jets is severe for top mass $m_t \sim m_W$. For masses below 70 GeV, a top signal could be separated from W signal because of the presence of events with njet ≥ 3. Other variables, not discussed above, that would be very useful are: the transverse mass $M_\perp$ (ev), the $\sum E_\perp$ in the event, the $\not{E}_T$ etc. A combination of these variables and the jet multiplicity, should allow detection of a top signal.

Finally, all above results were obtained with crude requirements on the jets. Effects of fragmentation, which make the definition of a jet difficult especially at low energies, and of underlying event, that contributes to the uncertainty in jet energy measurements, are quite important and have to be taken into account. We chose 15 GeV cuts on the jets in order to be in an energy region where these effects may not be too large. Studies of low energy jets in CDF are underway.

8.4 Summary

Preliminary studies show that the b background to a top signal in CDF can be reduced considerably by isolation cuts, especially for $P_T^e > 10$ GeV.

A preliminary study at the parton level with simple detector simulation shows that the W + jets background could be estimated for $m_t < 70$ GeV, whereas at $m_t \sim m_W$ detection of a top signal is going to be difficult.

More complete Montecarlo studies are needed for both types of backgrounds and are underway.

With the expected integrated luminosity in the 2-5 pb^{-1} range, Table 5 shows that CDF could be sensitive to top masses up to about 100 GeV. It is going to be a challenge if top really lies in the 70 - 100 mass region!

9.0 Summary

There will be a lot of data in the near future relevant to top searches. Present estimates of mass limits for the various detectors and accelerators are as follows:

	m_{top}
HERA	≤ 80 GeV
SLC-LEP	$\leq m_Z/2$
LEP II	≤ 90
UA2	≤ 70
UA1	≤ 100
CDF	≤ 100

REFERENCES

1. M. Gell-Mann, Phys. Rev. 125, 1067 (1962); Y. Ne'eman, Nucl. Phys. 125, 1067 (1962); S. Okubo, Prog. Theoret. Phys. 27, 949 (1962); M. Gell-Mann, Phys. Lett. 8, 214 (1964); G. Zweig, CERN Report 8182/Th. 401 (1964, unpublished); and CERN Report 8419/TH. 412 (1964, unpublished).

2. J. E. Augustin et al., Phys. Rev. Lett. 33, 1406 (1974); J.J. Aubert et al., Phys. Rev. Lett. 33, 1404 (1974).

3. G. Goldhaber et al., Phys. Rev. Lett. 37, 255 (1976); I. Peruzzi et al., Phys. Rev. Lett. 37, 569 (1976).

4. S. W. Herb et al., Phys. Rev. Lett. 39, 252 (1977).

5. M. Yamauchi, Proceedings of the XXIV International Conference on High Energy Physics, Munich (1988), p. 852. See also H. Kichimi, this conference.

6. C. Albajar et al. (UA1 Coll.), Z. Phys. C37, 505 (1988). See also this report.

7. G. Altarelli, M. Diemoz, G. Martinelli and P. Nason, Nucl. Phys. B303, 724 (1988).

8. N. Cabibbo, Phys. Rev. Lett. 10, 531 (1963).

9. M. Kobayashi and K. Maskawa, Prog. Theor. Phys. 49, 652 (1973).

10. H. Albrecht et al. (ARGUS Collaboration), Phys. Lett. 209B, 119 (1988); A. Jawahery, CLEO Collaboration, Proceedings of the XXIV International Conference on High Energy Physics, Munich (1988), p.545.

11. H. Burkhardt et al. (NA31 Collaboration), Phys. Lett. 206B, 169 (1988).

12. J. Ellis, J. Hagelin, S. Rudaz and D.D. Wu, Nucl. Phys. B304, 205 (1988); I.I. Bigi and A. I. Sanda, Phys. Lett. 194B, 307 (1987); H. Harari and Y. Nir, Phys. Lett. 195B, 586 (1987); G. Altarelli and P. Franzini, CERN-TH 4914/87 (Dec. 1987); V. Barger, T. Han, D.V. Nanopoulos and R.J.N. Phillips, Phys. Lett. 194B, 312 (1987) ; A. Datta, E.A. Paschos and V. Turke, Phys. Lett. 196B, 376 (1987); L.L. Chau and W.Y. Keung, University of California at Davis preprint UCD-87-02 (April 1987), unpublished.

13. A. Buras and J.M. Gerard, Phys. Lett. 203B, 272 (1988).

14. U. Amaldi et al., Phys. Rev. D36, 1385 (1987).

15. P. Nason, S. Dawson and R.K. Ellis, Nucl. Phys. B303, 607 (1988).

16. M. Diemoz, F. Ferroni, E. Longo and G. Martinelli, Z. Phys. C39, 21 (1988).

17. R.K. Ellis, "Heavy Quark Production at Collider Energies", in Proceedings of the 7th Topical Workshop on Proton-Antiproton Collider Physics, Fermilab, June 1988.

18. C. Albajar et al.,UA1 Collaboration, Phys. Lett. B213, 405 (1988).

19. G. A. Schuler, Nucl. Phys. B299, 21 (1988).

20. G. Ingelman, G.A. Schuler, Z. Phys. C40, 299 (1988).

21. R.A. Eichler, Z. Kunszt, Nucl. Phys. B308, 799 (1988) .

22. G. Ingelman, G.A. Schuler, J.F. de Troconiz DESY 88-143 submitted to Nucl. Phys. B.

23. E. Gabrielli, Mod. Phys. Lett. A1, 465 (1986).

24. J.H. Kuhn, A. Reiter and P.M. Zerwas, Nucl. Phys. B272, 560 (1986).

25. Proceedings of the 2nd MARKII Workshop on SLC Physics, SLAC-REPORT-306, Nov. 1986; Proceedings of the 3rd MARKII Workshop on SLC Physics, SLAC-REPORT-315, July 1987.

26. See for instance Sau Lan Wu, Physics Reports 107, Number 2-5, page 114-118 (1984).

27. Same as Reference 26, page 210-212.

28. G. Wormser, SLAC-PUB-4576 (1988).

29. A. Blondel, in "The Standard Model" Proc. 22nd Recontres de Moriond, Les Arcs, Savoie, 1987 (Editions Frontières, Gif-sur-Yvette, 1987), p.3; G. Costa et al., Nucl. Phys. B297, 244 (1988).

30. Figures obtained using EXPOSTAR, the electroweak Monte Carlo, by D.C. Kennedy, B. W. Lynn and C. J. - C. Im, SLAC Pub. 4128 (1988).

31. E. Keil, in Proc. ECFA Workshop on LEP 200, CERN 87-08, ECFA 87/108, p.17 (1987).

32. P. Igo-Kemenes et al., ibid.; p. 251.

33. W. Buchmüller et al., in Physics at LEP, CERN 86-02, p. 203 (1986).

34. F. Wilczek, Phys. Rev. Lett. 39, 1304 (1977).

35. This report is a condensed version of Ref. 32, to which all credit should go.

36. L. Di Lella, Lectures given at the Cargese Summer School, preprint CERN-EP/88-02 (1988).

37. J. Schacher, "Physics with ACOL at the CERN pp Collider", contribution to these proceedings.

38. C. Booth (UA2 Collaboration), "UA2 at ACOL", Proc. 6th Topical Workshop on Proton-Antiproton Collider Physics, Aachen, 1986 (World Scientific, Singapore, 1987), p.381.

39. M. Moniez, These d'Etat, LAL preprint, LAL 88-17 (1988).

40. UA1 Collaboration, CERN SPSC/83-48 and CERN SPSC/84-72; M.G. Albrow et al., Nucl. Instr. and Methos A265, 303 (1988); G. Bauer, "The UA1 Uranium-TMP Calorimeter", talk given at the 7th Topical Workshop on Antiproton-Proton Collider Physics, FNAL, June 1988.

41. a) P. Colas and D. Denegri, Phys. Lett 195B, 295 (1987); b) see also S. Gupta and D.P. Roy, Z. Phys. C39, 417 (1988); R. Kleiss et al., Z. Phys. C39, 393 (1988).

42. C. Albajar et al., UA1 Collaboration, Phys. Lett. 193B, 389 (1987).

43. C. Albajar et al., UA1 Collaboration, "Studies of Intermediate Vector Boson Production and Decay in UA1 at the CERN Proton-Antiproton Collider", CERN EP/88-168, November 29th 1988; C. Stubenrauch, "Etude de la Production de Bosons W et Z dans l'èxperience UA1", PhD thesis, Universitè de Paris-Sud (June 1987), note CEA-N-2532.

44. P. Bagnaia et al., UA2 Collaboration, Phys. Lett. 139B, 105 (1984).

45. R. Ansari et al, UA2 Collab., Phys. Lett. B194, 158 (1987).

46. G. Bauer et al., UA1 TN 87-09.

47. F. Halzen, C.S. Kim, S. Pakvasa, "The Standard Model with Three Generations: Closing in on the Top Quark Mass; MAD/PH/394 (Nov. 1987).

48. P.Colas et al., Z. für Physik C40,527 (1988).

49. C. Albajar et al., UA1 collaboration, Phys. Lett. B198,271 (1987).

50. See the reports of G. Bellettini and R. Bensinger in these Proceedings.

51. These plots were made using the Montecarlo program PAPAGENO, written and maintained by Ian Hinchliffe (Lawrence Berkeley Laboratory, University of California, Berkeley). It is a parton level Montecarlo that includes exact matrix elements for the higher order QCD processes, whenever available.

52. F. Herzog, Z. Kunszt, Phys. Lett. 157B, 430 (1985).

53. F. Abe et al., NIM A271, 387 (1988) and references therein.

54. F. Abe et al., "A measurement of W Boson Production in 1.8 TeV $\bar{p}p$ collisions", CDF Note 788 (Nov. 1988), submitted to Phys. Rev. Lett.

55. F. Paige and S. Protopopescu, BNL 38034 (1986).

56. F. Halzen, D.M. Scott, Phys. Rev. D18, 3376 (1978).

57. S.D. Ellis, R. Kleiss, W.J. Sterling, Phys. Lett. 154B, 435 (1985); J.F. Gunion, Z. Kunszt, Phys. Lett. 161B, 333 (1985).

58. G. Altarelli, R.K. Ellis, M. Greco, G. Martinelli, Nuclear Physics B246, 12 (1984); G. Altarelli, R.K. Ellis, G. Martinelli, Z Phys. C27, 617 (1985).

LAWRENCE BERKELEY LABORATORY
TECHNICAL INFORMATION DEPARTMENT
1 CYCLOTRON ROAD
BERKELEY, CALIFORNIA 94720